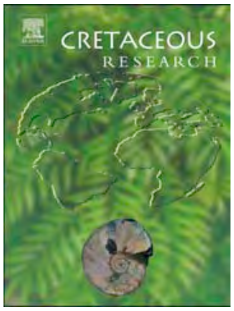

Taphonomy and palaeohistology of ornithischian dinosaur remains from the Lower Cretaceous bonebed of La Cantalera (Teruel, Spain)

Leire Perales-Gogenola, Javier Elorza, José Ignacio Canudo, Xabier Pereda-Suberbiola

PII: S0195-6671(18)30380-X

DOI: https://doi.org/10.1016/j.cretres.2019.01.024

Reference: YCRES 4072

To appear in: *Cretaceous Research*

Received Date: 19 September 2018

Revised Date: 20 December 2018

Accepted Date: 30 January 2019

Please cite this article as: Perales-Gogenola, L., Elorza, J., Canudo, J.I., Pereda-Suberbiola, X., Taphonomy and palaeohistology of ornithischian dinosaur remains from the Lower Cretaceous bonebed of La Cantalera (Teruel, Spain), *Cretaceous Research*, https://doi.org/10.1016/j.cretres.2019.01.024.

Taphonomy and palaeohistology of ornithischian dinosaur remains from the Lower Cretaceous bonebed of La Cantalera (Teruel, Spain)

Leire Perales-Gogenola[1*], Javier Elorza[2], José Ignacio Canudo[3,4], Xabier Pereda-Suberbiola[1]

(1) *Departamento de Estratigrafía y Paleontología, Facultad de Ciencia y Tecnología, Universidad del País Vasco/Euskal Herriko Unibertsitatea (UPV/EHU), Apartado de Correos 644, 48080 Bilbao, Spain. E-mail: leire.perales@ehu.eus*, xabier.pereda@ehu.eus*

(2) *Departamento de Mineralogía y Petrología, Facultad de Ciencia y Tecnología, Universidad del País Vasco/Euskal Herriko Unibertsitatea (UPV/EHU), Apartado de correos 644, 48080 Bilbao, Spain. E-mail: josejavier.elorza@ehu.eus*

(3) *Grupo Aragosaurus: Recursos geológicos y paleoambientes. IUCA, Paleontología, Facultad de Ciencias, Universidad de Zaragoza. 50009 Zaragoza, Spain. E-mail: jicanudo@unizar.es*

(4) *Museo de Ciencias Naturales, Universidad de Zaragoza, 50009 Zaragoza, Spain.*

* Corresponding author

ABSTRACT

The fossiliferous site of La Cantalera-1 (Teruel, Spain) has to date provided remains of more than 30 vertebrate taxa, including dinosaurs, crocodyliforms, pterosaurs, mammals, lizards, turtles, lissamphibians and teleosteans. Located in the lower part of the Blesa Formation (lower Barremian), it is one of the richest vertebrate-bearing deposits from the Lower Cretaceous of the Iberian Peninsula. In this work, taphonomic and palaeohistological studies are carried out on the basis of ornithischian (Ornithopoda and Ankylosauria) dinosaur samples in order to assess the diagenetic processes, to characterize the histological microstructures and, if possible, to make palaeobiological inferences about the state of maturation of the individuals. A variety of techniques are used in the taphonomic study, including scanning electron microscopy (SEM), cathodoluminescence (CL), X-ray diffraction (XRD) and ultraviolet fluorescence (UVF). The bone of the dinosaur samples has been converted into francolite (fluorapatite carbonate); the trabecular cavities are filled with semi-spherical forms of goethite and two different phases of calcite. In addition, the SEM and UVF techniques suggest the activity of coccoid-form bacteria and filaments of bacterial origin (biofilms?) in the bones, which possibly favoured fossilization. The dinosaur remains were subjected to fossil-diagenetic processes in a phreatic environment after a rapid burial, without appreciable seasonality effects. On the other hand, the palaeohistological study of both skeletal and dermal bones found in La Cantalera-1 shows a community of herbivorous dinosaurs composed mostly of immature ornithopods and at least one *Polacanthus*-like ankylosaur, as suggested by the organizational pattern of structural collagen fibres seen in some samples. The palaeobiological inferences drawn from this study support previous interpretations of a relative abundance of immature ornithischians in La Cantalera-1.

Keywords: fossil diagenesis; bone microstructure; Ornithopoda; Ankylosauria; Barremian; Iberian Peninsula.

1. Introduction

Our knowledge of the terrestrial ecosystems and especially the continental vertebrate faunas from the Early Cretaceous of Iberia has notably increased in recent years thanks to the discovery and study of rich fossiliferous outcrops (Ortega et al., 2006; Pereda-Suberbiola et al., 2012; Merino and Buscalioni, 2013). One of the most relevant localities of this age for its great biodiversity is the bonebed of La Cantalera-1, where more than thirty vertebrate taxa have been recognized up to now (Canudo et al., 2010). This site, located near the village of Josa (Teruel), has yielded a diverse accumulation of macro and micro-vertebrate fossil remains of Barremian age, including teleosteans, lissamphibians, turtles, lizards, crocodylomorphs, dinosaurs, pterosaurs and multituberculate mammals (Badiola et al., 2008; Canudo et al., 2010; Aurell et al., 2018 and references therein). Microfossils such as charophytes and ostracods are very abundant at La Cantalera-1; also frequent are plant fragments and continental gastropods.

Dinosaurs are a significant component of the vertebrate fauna from La Cantalera-1, since they represent more than half of the identified species (Canudo et al., 2010). The dinosaurs comprise ornithopods, ankylosaurs, sauropods and theropods, the latter being the most diverse clade in the number of species (Alonso and Canudo, 2016). Ornithopods are the most abundant dinosaur remains within the fossil assemblage (Ruiz-Omeñaca et al., 1997; Canudo et al., 2010). Based on teeth and postcranial remains, three different taxa of iguanodontian ornithopods have been identified, one of them related to *Delapparentia turolensis* Ruiz-Omeñaca, 2011 (Gasca et al., 2014). Moreover, a small basal ornithopod is also present. With regard to the ankylosaurian material, which includes isolated teeth, vertebral remains and osteoderms, this has been identified as belonging to a taxon close to the genus *Polacanthus* (Canudo et al., 2004, 2010).

This work is the first palaeohistological study of dinosaur fossil bones from La Cantalera-1. Ornithischian (both ornithopod and ankylosaur) remains are studied in order to ascertain the mineralogy and petrology of the samples as well as to reconstruct the taphonomic history of the site, to characterize the histological structures of the different tissues of the dinosaur bones, and thus to make palaeobiological inferences. A preliminary account of the palaeohistological features observed in the ornithischian dinosaur remains from La Cantalera-1 was recently published (Perales-Gogenola et al., 2018).

2. Geological setting

The vertebrate site of La Cantalera-1 (Teruel) is located in the Oliete sub-basin in the northwestern marginal areas of the Maestrazgo Basin (Iberian Range) (Fig. 1). The synrift sedimentation and synsedimentary extensional tectonics of the Oliete sub-basin have been summarized by Aurell et al. (2018). As noted by these authors, the Blesa Formation includes an up-to-150 m-thick siliciclastic-carbonate, continental-coastal succession that represents the onset of the Early Cretaceous synrift sedimentation in the Oliete sub-basin. The early Barremian age of this unit is well constrained by the occurrence of charophytes in some of the palustrine–lacustrine deposit intervals, and in particular by the presence of the clavatoracean *Atopochara trivolvis triquetra* in the lower levels of the Blesa Formation (Canudo et al., 2010, 2012; see Riveline et al., 1996). Two outcrops are known at La Cantalera-1 area: La Cantalera-1 includes a rich vertebrate accumulation consisting mainly of isolated teeth and disarticulated postcranial remains; eggshell fragments are also abundant (Moreno-Azanza et al., 2014). La Cantalera-2 is located about 500 m south from the classic site of La Cantalera-1 and is an outcrop laterally equivalent to it (Gasca et al., 2014).

In lithological terms, La Cantalera-1 comprises grey clays deposited in the lowest part of the Lower Blesa Sequence. Greyish and ochrish to reddish marls and clays with local root traces and nodulization are dominant in the lower part of this sequence, and represent distal alluvial to palustrine mudflat deposits with local sheet-flood and debris-flow deposits (Aurell et al., 2018). The relatively high calcium carbonate content in these facies reflects the composition of the drained area, which consists of Jurassic limestones and marls. Red pisolithic clays are also found in the lowermost part of the Lower Blesa Sequence, indicating lateritic soils on a Jurassic substratum (Aurell et al., 2018).

The taphonomic evidence suggests that the fossil association of La Cantalera-1 reflects a significant part of the biodiversity of a freshwater lentic ecosystem (Canudo et al., 2010). The site has been interpreted as a concentration of small, multitaxic vertebrate remains dominated by elements that are less than 5 cm in maximum dimension, i.e. a vertebrate microfossil assemblage (in the sense of Eberth and Currie, 2005). The assemblage includes partially articulated remains and disarticulated vertebrate debris. It was formed as an attritional deposit of bioclasts through progressive accumulation on a poorly drained floodplain (Canudo et al., 2010). In this low-energy depositional setting, preservational patterns vary and the vertebrate assemblage includes both autochthonous and parautochthonous elements, consisting almost exclusively of terrestrial and amphibious taxa that lived near the deposit area. There is no indication of significant transport, so the fossil assemblage can be regarded as a time-averaged sample of the source community (sensu Rogers and Brady, 2010), specifically the La Cantalera-1 wetland ecosystem (Moreno-Azanza et al., 2014). The site probably represents a marshy environment with periodic droughts, resulting in an intermittent body of water that periodically dried up (Canudo et al., 2010). The rich biodiversity of La Cantalera-1 may be due to the concentration of vertebrate remains into restricted flooded areas during dry seasons (Aurell et al., 2004). Furthermore, this small lacustrine area has been regarded as a feeding area for herbivorous dinosaurs (Ruiz-Omeñaca et al., 1997) and was presumably close to a nesting area, which could explain the abundance of small-sized individuals and the presence of fossil eggshells (Moreno-Azanza et al., 2014).

3. Material and methods

The material studied from the La Cantalera-1 site consists of twenty ornithischian fossils, including twelve fragmentary or incomplete bones (vertebrae, ribs, ossified tendons and two long bones) corresponding to Ornithopoda and eight dermal elements (including keeled scutes, small spines and ossicles; see Blows, 2001 for terminology) belonging to Ankylosauria (Table 1). This studied material comes from the erosion of the fossiliferous level and lack sings of transport. This selection was made according to the available material from the La Cantalera-1 site and the search for different palaeohistological microstructures in the different skeletal elements. The minimum number of individuals is unknown but we assume that all the individuals belonged to a single population. The material is housed in the Museo de Ciencias Naturales of the Universidad de Zaragoza (MPZ) (Canudo, 2018).

For the palaeohistological analysis, thin sections were obtained following the standard techniques for hard histological tissues described by Chinsamy and Raath (1992). The thickness of the sections was individually selected according to the characteristics of each piece, obtaining a thickness range of 30–50 µm. The description of the bone microstructures was undertaken using an Olympus BX41 petrographic microscope coupled to an Olympus CAMEDIA-C7070 photographic camera at the University of Zaragoza. The typological classification of Francillon-Vieillot et al. (1990) was followed. The images obtained were edited using Adobe Illustrator CS6®.

A selection of eleven petrographic thin sections of ornithischian fossil bones from La Cantalera-1 was prepared for standard transmitted light petrography and carbonate staining with Alizarin Red S and potassium ferricyanide (following Dickson, 1965). Polished sections were used for cathodoluminescence (CL). A number of samples were selected and examined under a scanning electron microscope (SEM), and also qualitatively determined (Al, Si, Fe, P, K, Ca) by energy-dispersive spectrometry (EDX) using a Jeol JSM-T6400 at the Universidad del País Vasco/Euskal Herriko Unibertsitatea (UPV/EHU). All CL work employed a Technosyn cold-cathode luminescence system, Model 8200 Mk II, mounted on an Olympus triocular research microscope with a maximum magnification capability of 400x using universal stage objectives. Standard operating conditions included an accelerating potential of 12 kV and a 0.5–0.6 mA beam current with a focused beam diameter of approximately 5 mm. The study of the ultraviolet fluorescence (UVF) of the fossil bone and filling phases (goethite and two calcite types) was carried out using Nikon UN2 PSE100 fluorescence power supply equipment attached to a Nikon Eclipse LV 100Pol microscope and a super high pressure mercury lamp power supply as the light source at the Instituto Geológico y Minero (IGME, Madrid). XRD analyses were performed with a Phillips PW1710 diffractometer using Cu Kα radiation monochromated by graphite with generator conditions of 40 kV, 20 mA, with a step size of 0.02° (°2θ) and a time per step of 1 s.

4. Results

4.1. Palaeohistology

The palaeohistological features of the ornithopod and ankylosaurian bones are described below separately (see Fig. 2-4).

4.1.1. Ornithopoda

Some fragmentary vertebrae (MPZ 2018/494, MPZ 2018/500 and MPZ 2018/501) and a neural arch (MPZ 2018/495) were studied. The vertebra thin sections show a great percentage of trabecular bone and a small portion of compact bone. The compact tissue is formed by a lamellar matrix and is variable between the samples. Some of them show bone deposited by a periosteum (MPZ 2018/501; Fig. 2A) or an external avascular layer (MPZ 2018/495; Fig. 2B). The vascularization ranges from a laminar orientation with abundant vascular channels (MPZ 2018/494; Fig. 2C) to a poor vascularization (MPZ 2018/501; Fig. 2A). Primary osteons (MPZ 2018/494; Fig. 2C), secondary osteons (MPZ 2018/500, MPZ 2018/495; Fig. 2B and D) and Haversian bone (MPZ 2018/501; Fig. 2A) are found in different samples. In general, the samples do not show periosteal zonation – except in the above-mentioned sample (MPZ 2018/501; Fig. 2A) – or LAGs (lines of arrested growth).

Sample MPZ 2018/501 presents bone that was deposited by a periosteum–composed of lamellar matrix with little or no vascularization (Fig. 2A). The preserved compact bone shows a great density of secondary osteons, superimposed upon one another, with longitudinal vascularization and Volkmann’s channels, a typical example of Haversian bone (Francillon-Vieillot et al., 1990) in which the primary lamellar matrix is almost not visible. The neural arch fragment (MPZ 2018/495; Fig. 2B and D) is composed of a larger percentage of trabecular bone than of compact bone. The compact part is composed of secondary osteons of variable size (Fig. 2B and D). There is an avascular layer without zonation or LAGs in the most external part of the compact bone (Fig. 2B).

The three fragmentary dorsal ribs (MPZ 2018/493, MPZ 2018/497 and MPZ 2018/499) show trabecular bone and fibrolamellar bone matrix. Primary osteons (MPZ 2018/492), secondary osteons (MPZ 2018/497) or both types (MPZ 2018/493) are observed in different samples. One of them shows weak lamination in the external cortex of the compact bone (MPZ 2018/493; Fig. 2E). This cortex is presented as an avascular layer with lacunae in a lamellar matrix (Fig. 2E). Lamination is not present in the rest of the compact tissue. The outer part of the inner compact bone shows scattered osteons with longitudinal vascularization and lamellar matrix. There are secondary osteons within trabeculae that extend through the medullary cavity, also in a l~~l~~amelar matrix (Fig. 2F). The rib MPZ 2018/499 (Fig. 2G-H) has a 50-50 proportion of trabecular (Fig. 2H) and compact bone (Fig. 2G), without external cortex. Within the compact tissue, two different types of structure can be observed in the internal and external faces of the rib. Two different colorations are visible in the bone (Fig. 2G). It is composed of longitudinal vascularization and of secondary osteons in a lamellar-fibrolamellar matrix. There are Volkmann’s channels that connect the osteons, which have well-defined resorption lines. MPZ 2018/492 (Fig. 3A-B) is an ornithopod rib, in which both the compact and trabecular bone are well preserved. The compact bone is formed by a lamellar matrix with high vascularization of simple channels in a random organization and scarce primary osteons (Fig. 3A). The transition from compact to trabecular bone is abrupt, from small vascular channels to large medullary cavities (Fig. 3B).

Two appendicular bones were studied, including an ornithopod ulna fragment (MPZ 2018/496) and an iguanodontoid fibula (MPZ 2018/502; Fig. 3C-E). The ulna (MPZ 2018/496) presents a higher proportion of trabecular tissue than of compact bone; no external cortex, zonation or LAGs are recorded. The compact bone, formed by a lamellar matrix, is composed of secondary osteons of different sizes that are overlapping due to the great density of vascularization (similar to Fig. 3C-D). In some parts of the section, Volkmann’s channels are seen connecting the osteons. The fibula (MPZ 2018/502; Fig. 3C-E) presents azonal compact bone with longitudinal vascularization. The compact bone represents a thicker layer than the trabecular tissue. It is composed almost entirely of secondary osteons with marked resorption lines. There are also Volkmann channels connecting the osteons. This is a typical example of Haversian bone.

The studied ossified tendons (MPZ 2018/491 and MPZ 2018/498; Fig. 3F) are also an example of dense Haversian tissue (Organ and Adams, 2005), with longitudinal vascularization and secondary osteons of different sizes (Fig. 3F). The concentric envelopes are formed by lamellar bone and the resorption lines are visible in the secondary osteons (Fig. 3F). The tissue presents the same structure in the entire tendon, but some parts of the section show a slightly lower density of osteons.

4.1.2. Ankylosauria

The dermal ossicles (MPZ 2018/506, MPZ 2018/507 and MPZ 2018/508) are formed by azonal primary lamellar bone with a great complexity of collagen structural fibres, which are parallel and perpendicular to the base of the ossicle, showing a more (MPZ 2018/508; Fig. 4A-D) or less (MPZ 2018/506) complex organization. The most characteristic feature of MPZ 2018/508 is the particular spatial organization of the collagen structural fibres; some are parallel to the base, and others perpendicular to the parallel ones, producing a pattern of bands (Fig. 4A-D). The vascularization of this particular tissue is high, with imbricated primary osteons in the collagen structural fibres. Some vascular channels open to the surface of the osteoderm, especially in the basal portion (Fig. 4E).

The dermal scutes are composed of trabecular bone and compact lamellar bone with collagen structural fibres. The proportion of trabecular to compact bone is variable among the different samples. A pattern of high spatial organization of the collagen fibres is observed (MPZ 2018/509, MPZ 2018/511). The presence of osteons is also variable. Some samples show scarce scattered osteons (MPZ 2018/509), whereas others present a great density of primary and secondary osteons (MPZ 2018/505; Fig. 4E). The outer cortex of the compact bone is an azonal lamellar matrix.

The small dermal spines studied here correspond to the distal end (MPZ 2018/503; Fig. 4G) and the basal part (MPZ 2018/504; Fig. 4H) of the spine. Some differences in the microstructure of both samples are seen. There is a gradual transition in both samples from the compact bone cortex to the trabecular cavities. This transition is more abrupt in the basal part (MPZ 2018/504) than at the distal end (MPZ 2018/503). The compact bone is composed of primary lamellar-fibrolamellar bone with primary osteons, wide vascular channels and collagen structural fibres. Inside the trabeculae of the trabecular bone, there are some deformed primary osteons and collagen fibres. There is neither zonation nor external wall of the compact bone well-preserved in any of the samples.

4.2. Taphonomy

In thin sections, the compact bone tissue shows a slight pink staining that affects both the part constituted by the secondary osteons and the primary matrix when it is treated with an Alizarin Red S stain and observed with plane-polarized light (parallel Nicols). In the primary matrix, osteocyte lacunae of greater dimensions and without apparent order persist in a high proportion, as opposed to the lacunae inside the secondary osteons, where they are smaller and show a concentric distribution with the lamellae of the osteons. Small, irregular fractures bleach the area of influence of the main fracture of the mineralizing fluids coming from them, whereas the Haversian channels, as well as parts of the Volkmann channels and the osteocyte lacunae, are completely filled by opaque ore (Fig. 5A).

The same surface with cross-polarized light (crossed Nicols) indicates the presence of a high density of secondary osteons formed by the concentric lamellae in the shape of a deformed Maltese cross, since the arms are not at 90° and the osteons have a major axis, whereas the rest of the bone matrix offers a very fine interlaced arrangement (MPZ 2018/502 T; Fig. 5B).

The primary osteons in the living animal are recognized by a central channel that contains two or more blood vessels, but lacks a cement line that delimits them (see Hall, 2005). When the passage from compact bone tissue to cancellous (trabecular) tissue is visible, a domain of pink staining is confirmed in the compact bone and subsequent bleaching, caused by a large fracture in the cancellous bone. The filling of the Haversian and Volkmann channels is predominantly formed by a clean carbonate without inclusions in the compact tissue, whereas in the cancellous tissue the opaque ore regularly upholsters the space of the medullary cavities between the trabeculae and is relieved by two carbonate phases (1, 2) until it occupies it completely (Fig. 5C-E).

The trabecular bone that makes up the cancellous tissue shows structural fibres by birefringence (MPZ 2018/496 T and MPZ 2018/500T; Fig. 5D-F). Exceptionally, the opaque ore that covers the medullary cavities can be altered, giving rise to opaque nuclei (g, goethite?), surrounded by oxidation alteration (h, hematite) (MPZ 2018/497 L; Fig. 5G-H).

Most of the thin sections observed present compact tissue with limited fracturing. When fracturing occurs, it corresponds to a type of fragile fracture perpendicular to the Haversian channels, with thin replacement veins formed by remobilization of the phosphatic phase, making the image cleaner to concentrate the insoluble remains at the limits of the lateral advancement (MPZ 2018/496 L; Fig. 6A). In more open fractures, replacement by iron oxides occurs in the compact bone, with irregular shapes conditioned by the original microstructure, advancing laterally towards the interior, slightly modifying its composition, but maintaining the original microstructure (MPZ 2018/499 L; Fig. 6B). In the cancellous/trabecular tissue, the crushing produced by early compaction is intense, with an accumulation of angular fragments that occupy the empty medullary spaces with the carbonated phase (there are no ores here) (MPZ 2018/510 T; Fig. 6C).

The filling of the medullary spaces between trabeculae that occurs in the cancellous tissue follows a regular pattern. The first thing that is deposited is a thin phase of opaque ore (besides the iron oxides), which covers all the available space with a growth towards the central zone of the hollow, recognized by small sub-spherical forms (goethite). This is followed by a filling of two differentiated carbonated phases; the first one (1) of clean equant crystals, and the second one (2), similar to the previous one but dirty in appearance, with insoluble iron oxides together with organic remains (MPZ 2018/496 L; Fig. 6D).

A special feature occurs when the cancellous bone is also mineralized by a replacement phase of iron oxides in bands that follow the shape of the cavity. This phase advances from contact with the opaque ore to the interior of the bone in a process of replacement; neither dissolution nor the subsequent filling (permineralization) is present, as can be seen with parallel and crossed Nicols (Fig. 6E-F). This replacement, more or less concentric to the shapes of the empty spaces, appears to be cut off abruptly and irregularly when observed with a greater magnification (Fig. 6G-H).

The microstructure of the ankylosaurian osteoderms is very different from what has been described in the compact and cancellous tissue of the ribs, vertebrae and long bones of ornithopods.

By staining with Alizarin Red S, it can be seen that the bone tissues are initially pink (p), with a subsequent bleaching stage (b) favoured by the presence of very fine fractures (Fig. 7A). Initially, they are composed of a compact tissue with bands of fibres parallel to each other, which intersect perpendicularly as a network with the scattered Volkmann channels occupied by large crystals, mostly of calcite, but with evidence of opaque ores that are very thin in relation to the ornithopod samples (MPZ 2018/509 L; Fig. 7B).

It is interesting to note that the filling of the empty spaces in the cancellous tissue is mostly carbonated (1), with just a remnant of the earliest phase of iron oxides (MPZ 2018/511 T and MPZ 2018/509 T; Fig. 7C-F).

Under cathodoluminescence (CL), the thin sections studied provide some details. Neither compact nor cancellous tissues are luminescent, although they can be differentiated from opaque ores that are blacker than tissue. In the filling, a luminescent behaviour is visible by differentiating the two recognized carbonate phases. The earlier phase formed by large crystals of clean equant calcite, with parallel Nicols, shows a certain arrangement in its growth, where there is a non-luminescent dark zone with straight rectilinear faces, followed by alternating reddish and yellow laminar growth, and finishing with a larger irregular area of yellowish tones. There can be considered to be regular growth with well-marked areas in this phase. In the later carbonated phase formed by calcite crystals with inclusions of insoluble remains, the luminescence is massively reddish, but not intense, with some yellow areas irregularly arranged and of small size. No order can be described in the growth of carbonated cement in this later phase (MPZ 2018/496 T; MPZ 2017/497 T; Fig. 8A-D).

Under ultraviolet fluorescence (UVF), the different late modifications undergone by the bone tissue are better appreciated. It is relevant to note that, just as with parallel Nicols the bone periphery and fracture zones did not show the staining in a pink tone, under UVF they show a strong light blue luminescence that advances towards the interior of the previously diagenetized bone. The filling of the trabecular spaces with goethite appears inert whereas the filling formed by clean calcite crystals from the first phase (1) is sensitive, with an intense dark blue luminescence. The second phase calcite (2) appears as non-luminescent, with some points irregularly distributed in a blue tone (Fig. 8E-F). In some sections, the bone structure undergoes a greater degree of alteration, leaving the entire surface practically in a light blue tone, whereas the remaining, unaffected part appears dark coloured (Fig. 8G-H).

5. Discussion

5.1. Palaeohistology

5.1.1. Ornithopoda

Among the studied samples of Ornithopoda there is great variability among the palaeohistological microstructures. Poorly organized but abundant vascularization, the presence of primary osteons and the absence of zonation or an external fundamental system (EFS), and a succession of LAGs very close to each other (Francillon-Vieillot et al., 1990), constitute the pattern seen in many of the samples. This pattern relates to immature individuals (Chinsamy-Turan, 2005; Padian and Lamm, 2013). At the same time, the secondary remodelling as Haversian bone seen in ossified tendons, some vertebrae and the long bones of other individuals indicates a more mature growth state (Fig. 2A and C, 3C-D) (Chinsamy-Turan, 2005).

The vertebral elements show a great proportion of trabecular bone except in one sample (MPZ 2018/501) (Fig. 2A). In general, the compact tissue does not show zonation or an external cortical complex that would indicate cyclicity in its growth or a mature state. The vascularization varies from primary osteons to dense Haversian tissue. Although it could be said that those individuals with greater vascular complexity, such as MPZ 2018/495 (Fig. 2B and D), would be in a state of more advanced growth than those with less complexity (e.g., MPZ 2018/494; Fig. 2C), the only thing that can be affirmed with certainty is that they would not have reached the adult state.

The dorsal ribs are formed from a previous cartilage mould whereas the cervical ribs are formed from the ossification of tendinous elements anchored to the caudal portion of the original cervical rib (Cerda, 2009, Zweers et al., 1987, Wedel et al., 2000). The general palaeohistology of MPZ 2018/493 is summed up as lax Haversian tissue and an avascular outer layer (Fig. 2E). The absence of a cortical complex indicates a subadult growth state in the individual. The presence of secondary osteons in MPZ 2018/497 points to secondary remodelling of the internal tissue, which is usually increased during growth (Chinsamy-Turan, 2005), but it is not possible to define the state of maturity of the individual. High vascularization of simple channels in the compact bone, seen in MPZ 2018/492 (Fig. 3A-B), indicates a potentially high growth rate and, along with the absence of LAGs, is an indicator of bone immaturity. Given the absence of LAGs or any other signs of a slower growth rate, sample MPZ 2018/499 (Fig. 2G) can be assumed not to have reached a mature state.

Ossified tendons are anatomically associated with the neural spines of the dorsal and caudal vertebrae, giving support to the tail. The presence of this kind of tendon is a typical feature of Ornithopoda (Sereno, 1997). Samples MPZ 2018/491 (Fig. 3F) and MPZ 2018/498 are composed of dense and lax Haversian tissue, respectively. The presence of this type of secondary tissue usually increases with age (Chinsamy-Turan, 2005; Klein and Sander, 2008).

Secondary remodelling may also be found in subadult bones, such as in the medium-sized dryosaurid *Dryosaurus* (Chinsamy, 1995). Given the palaeohistological features of the studied material from La Cantalera-1, most of the samples do not show signs of being at an adult stage.

5.1.2. Ankylosauria

The palaeohistological features differ with the type of dermal bone, i.e. keeled scutes, ossicles and small spines. These differences are related to the distinct functions that these elements may fulfil. The ossicles act as lightweight armour, and the scutes and spines are anatomical elements that probably served for exhibition or thermoregulation (Hayashi et al., 2010).

In the ossicles (Fig. 4A-D), a pattern in the distribution and orientation of the collagen structural fibres is observed, which is assumed to provide these dermal elements with hardness for their function as defensive armour (Scheyer and Sander, 2004). It has been shown that the density and distribution of these collagen fibres differ among the ankylosaurs, including ankylosaurids and nodosaurids (Hayashi et al., 2010). The studied ossicles (MPZ

2018/506, MPZ 2018/507 and MPZ 2018/508) are entirely composed of compact primary lamellar bone, without LAGs and with abundant collagen fibres. The structure formed by these fibres in MPZ 2018/508 (Fig. 4A-D) matches that described by Scheyer and Sander (2004) for *Polacanthus foxii*, although in MPZ 2018/508 the thick portion of trabecular bone is absent. Canudo et al. (2010) described the presence of an ankylosaur close to *Polacanthus* at La Cantalera-1 on the basis of isolated teeth. The three samples studied here show vascular channels that open to the surface of the osteoderm, probably accomplishing irrigation functions for the osteoderm and surrounding tissues. These vascular channels could be an indicator of active growth, and of a necessity for maintenance and reparation of the tissue (Curry, 1999; Sander et al., 2006). These channels may also indicate a role as a thermoregulator (Farlow et al., 2010).

With regard to MPZ 2018/509, the structural organization of the collagen fibres matches with that described for MPZ 2018/508 and therefore with the structures seen in *Polacanthus foxii* (Scheyer and Sander, 2004). In this case, the sample presents scarcely developed trabecular tissue, and the features of the compact bone suggest that, like MPZ 2018/506, MPZ 2018/507 and MPZ 2018/508, the dermal scute has not reached its mature state. The variation seen in the palaeohistological structure from the base to the tip in the small dermal spine is due to the different requirements of vascularization, as seen in the dorsal dermal plates of the stegosaur *Stegosaurus* (Buffrénil et al., 1986).

Vascularization is abundant in all the ankylosaurian samples. Continuous blood irrigation would have been necessary in the reparation and maintenance of the osteoderms in Ankylosauria and other thyreophorans, as is observed in *Stegosaurus* (Farlow et al., 2010), and this is evidenced by the external appearance and the histology of the dermal bones (Scheyer and Sander, 2004; Hayashi et al., 2009, 2010). Therefore, it is plausible that all types of osteoderms in Thyreophora played at least a minor role in thermoregulation (Farlow et al., 2010).

In general, the described palaeohistological features do not indicate a mature state of growth. Nevertheless, a subadult state cannot be assured either. There is a delay between the maturation of skeletal and dermal bones in Ankylosauria (Hayashi et al., 2009). This delay in the maturation of dermal bones is also known in other thyreophorans, such as *Stegosaurus* (Hayashi et al., 2009), and in extant reptiles (Vickaryous et al., 2001; Vickaryous and Hall, 2008).

5.2. Taphonomy

5.2.1. Generalities

Initially, a recent bone is composed by weight of 70% phosphate minerals (60% hydroxyapatite and 10% other phosphate minerals), 18% collagen as the main protein, 9% water, and 3% other proteins, lipids and mucopolysaccharides (glycosaminoglycans) (Pfretzschner, 2004). During fossil diagenesis, the proteins are more or less eliminated and replaced by inorganic substances. The hydroxyapatite [$Ca_5(PO_4)_3(OH)$] is modified by recrystallization and by the substitution of OH^- and PO_4^{3-} by Cl^-, F^- and CO_3^{2-}. In this way, it becomes a carbonate fluorapatite called francolite [$Ca_5(PO_4,CO_3)_3(F)$], this being the most stable mineral phase. In addition, Ca^{2+} in apatite can be replaced by metal ions such as Fe^{2+}, U^{4+}, Zn^{2+}, Mn^{2+}, Sr^{2+}, Ba^{2+} and others from the active diagenetic fluids (see Pfretzschner, 2004 and references therein). In extreme cases, the complete mineralogical replacement of the bone by pyrite or chalcedonite may occur, or even its complete dissolution, fundamentally due to the aggressiveness of the percolating ground waters (Barker et al., 1997). A recent study using laser-induced breakdown spectroscopy (LIBS) has determined the presence of lanthanides (Eu, Gd, La, Nd and Sm) in some crocodile and turtle fossils from this site (Anzano et al., 2017).

The stage of early diagenesis is considered to end when the replacement of the primordial collagen by minerals is completed and the fossil-diagenetic process undergone by the bone begins. In both stages, mineral formation can take place in the porous spaces of the bone, although most bones remain compact and external reagents can only enter the bone by diffusion (Pfretzschner, 2004). The Haversian channels are the main routes of diffusion, since they are generally arranged parallel to the long axis of the bone and are interconnected with Volkmann's channels. There does not seem to be a significant flow of fluids through the narrow lacunae of the osteons, nor through the tiny existing canaliculi. There is an even greater obstacle to diffusion flow when the secondary osteons, generated during the diagenetic process and arranged around the Haversian channels, are surrounded by a compact mineral wall known as the cement line (Hall, 2005). Diffusion can hardly extend beyond this line present around each secondary osteon. As a result, diffusion through the bone is a very slow and limited process. In early diagenesis, the replacement of collagen by minerals begins with the process of gelatinization, which is strongly influenced by pH, being considerably faster with a high pH than with a neutral pH (see the extensive work of Pfretzschner, 2004 for more details). The increased gelatinization of the collagen allows greater hydration of the protein, whereas fresh collagen contains only small amounts of water. The hydration of the gelatinized collagen swells the bone considerably (Walrafen and Chu, 2000). This swelling causes a characteristic pattern of microcracks in the Haversian channels. As a consequence, the bone material in a secondary osteon swells more quickly than in the remote regions, causing tension in the cement line surrounding each secondary osteon (Pfretzschner, 2004).

Experimentally, the so-called recrystallization window has been established, involving restricted chemical conditions and a narrow alkaline pH range, in which a bone can recrystallize from carbonated apatite to authigenic apatite (Berna et al., 2004). Thus, a small pH change in the medium dictates the rules of bone conservation. A bone in sediments in which the pore solution has a high pH (> 8.1) is likely to be better preserved: for instance, in a solution saturated with calcite. In the transition from alkaline to neutral conditions, the mineral component of the bone will be conserved, but affected by recrystallization. When the pH of the fluids retained in the sediment decreases (< 7), the bone will tend to dissolve rapidly (Berna et al., 2004).

5.2.2. Pink stains

When observed with parallel polars and stained by Alizarin Red S, the thin sections of the ornithopod and ankylosaur fossil bones from La Cantalera-1 show soft pink tones that suggest the incorporation of carbonate into the initial microstructure, both in the compact bone and in the cancellous tissue (Fig. 4A, C; Fig. 6A, C, E, G). As mentioned above, the bones are originally formed by hydroxyapatite [$Ca_5(PO_4)_3(OH)$], and during fossil diagenesis this can change to dahllite [$Ca_5(PO_4,CO_3)_3(OH)$] or to francolite [$Ca_5(PO_4,CO_3)_3(F)$], with an important contribution of carbonate in both cases. If the existing (OH^-) in the microstructure of the dahllite is replaced by (F^-) in quantities greater than 1% by weight, the compound is considered francolite (Hubert et al., 1996, Trueman, 1999, Elorza et al., 1999). On the other hand, the degree of substitution and mineralization within the PO_4^{-3} network varies with the type of bone, age and burial conditions during diagenesis (Timlin et al., 2000). For all these reasons, it seems logical to observe this soft pink stain, which is indicative of the presence of carbonates, since the XRD analysis indicates the diagenetic transformation to francolite as the final resulting mineral (Table 2). The fractures and the subsequent generation of veins produce a bleaching that suggests at least one modification, with a change towards neutral values in the pH, with the loss of previously acquired carbonate in the bone microstructure

(Fig. 6A-B). This selective absence of coloration indicates a late recrystallization forming authigenic apatite without enough carbonate, with the higher degree of crystallinity already commented on by Berna et al. (2004). In Table 1, the values obtained in the samples from La Cantalera-1 are compared with the francolite values given by Jarvis (1992) in his work on the phosphatic chalks used as a standard, together with the values provided by Elorza et al. (1999) based on dinosaur fossils from the Late Cretaceous site of Laño (Basque-Cantabrian Region).

Commonly used in the study of carbonate petrology (see Jackson et al., 2010; Rosales et al., 2018 and references included in both works), epifluorescence microscopy has been used to determine the presence of residual organic matter in a variety of fossil marine invertebrates, since the remnant organic matter in fossil specimens fluoresces brightly despite diagenesis, thereby revealing its distribution. This often allows discrimination of primary features that are otherwise obscured by neomorphism. The technique is rarely employed in the study of vertebrate fossil bones and fossil eggs containing embryonic remains (Jackson et al., 2010). We have not found any previous reference in the literature to cases where the diagenetic alteration generated in dinosaur bones as a product of bacterial activity has been pinpointed by UVF images. In our case, under UVF the fractures are indicated by a luminescence in a light blue tone, which determines the presence of residual organic matter (Fig. 8E-H). It seems that this delayed fracturing is the result of bacterial activity, also detected by the SEM in the collagen zone, which shows the presence of widespread, more or less spherical bodies ranging in size from 100-300 nm (Fig. 9A-H). These bodies could represent the relicts of nanobacterial cells (Russo et al., 2006).

5.2.3. Deformation

The secondary osteons display the shape of a Maltese cross with cross-polarized light, but the arms do not form the usual right angle; this may be indicative of having undergone crushing due to the compaction of the lamellae or simply because of the obliquity of the section. The compaction is more clearly reflected in the compact tissue by the presence of small fractures without displacement (Fig. 6A-B). In the cancellous tissue, there is occasionally a significant collapse and accumulation of angular fragments, similar to chaotic sedimentary breccia. Fractures have apparently occurred after filling by iron oxides (Fig. 6C). The fractures are refracted when they reach the goethite α-FeO (OH) filling, changing their direction and surrounding it. That is, the bone behaves in a fragile way, whereas the filling of ore and carbonate is more plastic (Fig. 7C, E, G). The small radial cracks that characteristically run across the cement lines of secondary osteons due to the gelatinization of the existing collagen (Pfretzschner, 2004) are here not observed.

Hubert et al. (1996) interpreted the generalized fracturing of bones as evidence of trampling by large animals before they were buried. This explanation does not seem plausible because such fractures are also found in bones deposited in marine sediments. Therefore, a diagenetic origin due to overload pressure should be assumed as the most plausible origin for these structures. The compact bone parts are more affected by cracking than the cancellous bone parts, probably because the latter bone structure is more flexible under a weak initial burial pressure than compact bone, but tends to collapse completely and break under compaction with a higher pressure.

5.2.4. Fillings

When bone maintains its microstructure and the fluids of the medium reach the intertrabecular spaces, a filling occurs with numerous and probably rapid Eh and pH fluctuations, in addition to the variation in the pore water fluid composition (Barker et al., 1997; Pfretzschner, 2004). The intertrabecular mineral deposits identified in La Cantalera-1 seem to operate with a certain independence from each other. They preserve the histological structures and follow slightly different patterns, despite being separated from each other by only a few millimetres (Fig. 9A-B). It seems that the precursor mineral is initially ferrihydrite [$Fe^{3+}{}_{10}O_{14}(OH)_2$], which in precise diagenetic conditions becomes a dominant phase of goethite α-[FeO(OH)] (Table 2). The filling of the empty spaces is completed with two different phases of calcite (Fig. 5C-F). There is no evidence of the presence of pyrite (FeS_2) reflected by light microscopy or by XRD. Pyrite can be formed during early diagenesis due to the favourable reducing conditions that are produced by high pH values and a low redox potential (pH 8, Eh <-230mV), since the decomposition of collagen contributes H_2S to the medium (see Pfretzschner, 2000, 2001, 2004 for more details).

By contrast, under aqueous oxidizing conditions the possible oxide precursor (ferrihydrite) tends to become goethite and/or hematite during early diagenesis, because these phases are thermodynamically more stable (Kremer et al., 2012; see also Cudennec and Lecerf, 2006; Parenteau and Cady, 2010; Das et al., 2011). When a process of dehydration occurs at low temperatures, goethite becomes hematite (Faria and Lopes, 2007), although the mineralization of bacterial aggregates does not exclude the initial formation of both hematite and goethite. The precipitation of both minerals, always starting from ferrihydrite as a precursor, is favoured by an increase in temperature and pH. Thus, it seems that hematite is formed under neutral or slightly alkaline conditions (pH 7-9), whereas goethite predominates when the pH values are outside this range, being present mostly when the concentration of ions (Fe^{3+}) grows in equilibrium with ferrihydrite, whereas hematite is more abundant when the ions (Fe^{3+}) decrease in concentration (Schwertmann and Murad, 1983).

In our case, goethite (detected by XRD and SEM-EDX) is the majority component in parallel laminar forms just in contact with the bone, passing to radial proto-botryoidal endings (Fig. 9C-E). The presence of hematite (Fe_2O_3) was not detected using X-ray diffraction.

The older calcite is superimposed on the botryoidal forms of the diagenetic goethite (Fig.

9E). Such calcite appears clean and without inclusions, whereas the second phase of calcite, which often leaves empty spaces unoccupied, is characterized by its dirty appearance with parallel polars due to the numerous irregular and opaque inclusions that it encompasses (organic matter and oxides). The behaviour in CL is well differentiated in this sense and determines a first oxidant phase without luminescence (comprising the beginning of calcite precipitation with regular growth edges), which becomes a reducing environment in a part of the clean calcite with zoned growth and all the calcite presenting inclusions, where the luminescence in red is homogeneous and where it has not been possible to determine compositional zoning (Fig. 8A-D). This behaviour suggests a depositional environment with rapid burial and cementing already achieved in the phreatic zone, since there is no evidence of microstructures typical of a vadose environment, such as meniscus, pendant or geopetal cements. The filling process does not necessarily occur in the same sequence in all the cavities, which is indicative that there is not a sufficiently fluid communication between the Haversian-Volkmann channels to give a single pattern. This is symptomatic of how in compact tissue the fillings sometimes occur only with opaque ore and at other times with calcite, whereas in cancellous tissue the pattern is more uniform, with the representation of the early phase of goethite and two later phases of calcite (Fig. 4C-F, 5D-H). It seems that these fillings are not spaced in time, since there are no interruptions long enough to generate contractions due to the lack of fluids (mud-crack patterns in clays). All these features are typical of burial in a phreatic environment, without seasonal effects that could make the water sheet fluctuate (hydromorphic soil?). It is generally accepted that diagenetic goethite is formed under cool/wet conditions in soils rich in organic matter, whereas hematite is formed under warm/dry conditions in soils poor in organic matter (Bao et al., 1998).

Also unique is the advance in concentric forms, sometimes with abrupt endings, of the iron oxides on the concentric lamellae of the cancellous tissue. This is indicative of a diffusion process through the bone microstructure under favourable conditions, without affecting it, as occurs if the pH conditions are lower (Barker et al., 1997) (Fig. 6E-H).

Finally, there is evidence of subsequent microbial participation, mainly in the collagen bundles and the fractures mineralized by francolite, but also during the formation of goethite and calcites, as can be seen in the images provided by UVF and SEM (Fig. 8E-H, 9A-H). The observed coccoid shapes are similar in size (100-300 nm) and distribution to those described in the ultrastructure of tadpole soft tissue and supposed coprolithic material (Toporski et al., 2002), as well as those associated with the skull of a tapejarid pterosaur (Pinheiro et al., 2012) and with the syndepositional fibrous cements (evinosponges) found in the Middle Triassic dolomites of Italy (Russo et al., 2006).

7. Conclusions

A taphonomic and palaeohistological study of dinosaur fossil bones from the Barremian bonebed of La Cantalera-1 (Teruel) is presented. This site is one of the most significant Lower Cretaceous vertebrate localities in Spain on account of its biodiversity, having yielded fossil remains of more than thirty vertebrate species, including dinosaurs, crocodyliforms, pterosaurs, mammals, lizards, turtles, lissamphibians and teleosteans.

The palaeohistological study of ornithischian samples from La Cantalera-1 shows a great range of microstructures among Ornithopoda, corresponding mostly to immature individuals. The characteristic pattern observed in the dermal bones, especially the spatial organization of collagen structural fibres, allows the presence of a *Polacanthus*-like ankylosaur to be recognized. Based on the dermal samples, the occurrence of a second ankylosaur in La Cantalera-1 cannot be ruled out. The palaeohistological results support previous interpretations of the relative abundance of immature ornithischian individuals in this site, including juvenile to subadult ornithopods and it is coherent with the initial palaeoecological interpretation of Cantalera-1 as feeding area (Ruiz-Omeñaca et al., 1997).

The petrological study indicates that the bone mineral in the dinosaur samples from La Cantalera-1 has become francolite (carbonate fluorapatite), with a sufficient carbonate contribution to stain in a pale pink tone and a regular appearance in the compact and cancellous (trabecular) bone tissue. Subsequent fracturing modified this composition by bleaching the area of influence. The filling of the intertrabecular spaces is produced by hemispherical forms of fibro-radial goethite and two different phases of calcite. By means of scanning electron microscopy (SEM) and ultraviolet epifluorescence (UVF), bacterial activity can be verified with the formation of coccoid carpets and filaments in the bones themselves, fractures and, to a lesser extent, in the filling phases. The textural relationships of the mineral filling suggest that the studied remains underwent rapid burial, without appreciable seasonal effects, and quickly reached the phreatic environment where the described fossil-diagenetic processes took place.

Acknowledgements

This research work has been financed by the project CGL2017-85038-P of the Spanish Ministerio de Economía y Competitividad and the European Regional Development Fund. LPG and XPS are supported by the Gobierno Vasco/Eusko Jaurlaritza (research group IT-1044-16) and by the Universidad del País Vasco/Euskal Herriko Unibertsitatea (UPV/EHU, research group PPG17/05); JIC is supported by the Gobierno de Aragón (Grupos de Referencia); JE is supported by the Fundación Elorza. LPG has received a pre-doctoral grant from the UPV/EHU. We thank Dr. I. Rosales (IGME, Madrid) for her invaluable help in obtaining epifluorescence images. We are also grateful to Rupert Glasgow for editing the English text. We thank the two anonymous reviewers and the editor (Dr. Eduardo

Koutsoukos), whose valuable comments and suggestions have helped improve this manuscript.

References

Alonso, A., Canudo, J.I., 2016. On the spinosaurid theropod teeth from the early Barremian (Early Cretaceous) Blesa Formation (Spain). Historical Biology 28(6), 823–834.

Anzano, J.M. Lasheras, R.M., Cajal, J., Paulés, D., Sánchez, T. Escudero, M., Canudo, J.I. 2017. Determination of Lanthanides in fossil samples using laser induced breakdown spectroscopy. Journal of the Chemical Society of Pakistan 39(4), 516–523.

Aurell, M., Bádenas, B., Canudo, J.I., Ruiz-Omeñaca, J.I., 2004. Evolución tectosedimentaria de la Fm. Blesa (Cretácico Inferior) en el entorno del yacimiento de vertebrados de La Cantalera (Josa, Teruel). Geogaceta 35, 11–14.

Aurell, M., Soria, A.R., Bádenas, B., Liesa, C.L., Canudo, J.I., Gasca, J.M., Moreno-Azanza, M., Medrano-Aguado, E., Meléndez, A., 2018. Barremian synrift sedimentation in the Oliete sub-basin (Iberian Basin, Spain): Palaeogeographical evolution and distribution of vertebrate remains. Journal of Iberian Geology 44, 285–308.

Badiola A., Canudo J.I., Cuenca-Bescós G. 2008. New multituberculate mammals of the Hauterivian/Barremian transition of Europe (Iberian Peninsula). Palaeontology 51(6), 1455–1469.

Bao, H., Koch, P.L., Hepple, R.P., 1998. Hematite and calcite coatings on fossil vertebrates. Journal of Sedimentary Research A 68, 727–738.

Barker, M.J., Clarke, J.B., Martill, D.M., 1997. Mesozoic reptile bones as diagenetic windows. Bullétin de la Société géologique de France 168, 535–545.

Berna, F., Matthews, A., Weiner, S., 2004. Solubilities of bone mineral from archaeological sites: the recrystallization window. Journal of Archaeological Science 31, 867–882.

Blows, W.T., 2001. Dermal armor of the polacanthine dinosaurs. In: Carpenter, K. (Ed.), The Armored Dinosaurs. Indiana University Press, Bloomington, pp. 363–385.

Buffrénil, V. de, Farlow, J.O., Ricqlès, A. de, 1986. Growth and function of *Stegosaurus* plates: Evidence from bone histology. Paleobiology 12, 459–473.

Canudo, J.I., 2018. The collection of type fossils of the Natural Science Museum of the University of Zaragoza (Spain). Geoheritage 10, 385–392.

Canudo, J.I., Ruiz-Omeñaca, J.I., Cuenca-Bescós, G., 2004. Los primeros dientes de anquilosaurio (Ornithischia: Thyreophora) descritos en el Cretácico Inferior de España. Revista Española de Paleontología 19, 33–46.

Canudo, J.I., Gasca, J.M., Aurell, M., Badiola, A., Blain, H.A., Cruzado, P., 2010. La Cantalera: an exceptional window onto the vertebrate biodiversity of the Hauterivian–Barremian transition in the Iberian Peninsula. Journal of Iberian Geology 36, 205–224.

Canudo, J.I., Gasca, J.M., Moreno-Azanza, M., Aurell, M., 2012. New information about the stratigraphic position and age of the sauropod *Aragosaurus ischiaticus* from the Early Cretaceous of the Iberian Peninsula. Geological Magazine 149, 252–263.

Cerda, I. A., 2009. Consideraciones sobre histogénesis de las costillas cervicales en los dinosaurios saurópodos. Ameghiniana 46, 193–198.

Chinsamy, A., 1995. Ontogenetic changes in the bone histology of the Late Jurassic ornithopod *Dryosaurus lettowvorbecki*. Journal of Vertebrate Palaeontology 15, 96–104.

Chinsamy, A., Raath, M.A., 1992. Preparation of fossil bone for histological examination. Palaeontologia Africana 29, 39–44.

Chinsamy-Turan, A., 2005. The Microstructure of Dinosaur Bone: Deciphering Biology witht Fine-Scale Techniques. Johns Hopkins University Press, Baltimore and London, 216 pp.

Cudennec, Y., Lecerf, A., 2006. The transformation of ferrihydrite into goethite or hematite, revisited. Journal of Solid State Chemistry 179, 716–722.

Curry, K.A., 1999. Ontogenetic histology of *Apatosaurus* (Dinosauria: Sauropoda): new insights in growth rates and longevity. Journal of Vertebrate Paleontology 19, 654–665.

Das, S., Hendry, M.J., Essilfie-Dughan, J., 2011. Transformation of two-line ferrihydrite to goethite and hematite as a function of pH and temperature. Environmental Science and Technology 45, 268-275.

Dickson, J.A.D., 1965. A modified staining technique for carbonates in thin section. Nature 205, 587.

Eberth, D.A., Currie, P.J., 2005. Vertebrate taphonomy and taphonomic modes. In: Currie, P.J., Koppelhus, E.B. (Eds.), Dinosaur Provincial Park. A Spectacular Ancient Ecosystem Revealed. Indiana University Press, Bloomington, pp. 453–477.

Elorza, J., Astibia, H., Murelaga, X., Pereda-Suberbiola, X., 1999. Francolite as a diagenetic mineral in dinosaur and other Upper Cretaceous reptile bones (Laño, Iberian Peninsula): microstructural, petrological and geochemical features. Cretaceous Research 20, 169–187.

Faria, D.L.A. da, Lopes, F.N., 2007. Heated goethite and natural hematite: can Raman spectroscopy be used to differentiate them? Vibrational Spectroscopy 45, 117–121.

Farlow, J., Hayashi, S., Tattersall, G.J., 2010. Internal vascularity of dermal plates of *Stegosaurus* (Ornithischia, Thyreophora). Swiss Journal of Geosciences 103, 173–185.

Francillon-Vieillot, H., Buffrénil, V. de., Castanet, J., Géraudie, J., Meunier, F.J., Sire, J.Y., Zylberberg, L., Ricqlès, A de., 1990. Microstructure and mineralization of vertebrate skeletal tissues. In: Cartes, J.G. (Ed.), Skeletal Biomineralization: Patterns, Processes and Evolutionary Trends. Van Nostrand Reinhold, New York, pp. 471–530.

Gasca, J.M., Canudo, J.I., Moreno-Azanza, M., 2014. On the Iberian iguanodont dinosaur diversity: New fossils from the lower Barremian, Teruel province, Spain. Cretaceous Research 50, 264–272.

Hall, B. K., 2005. Bone and cartilage: developmental and evolutionary skeletal biology. Elsevier Academic Press, London, 760 pp.

Hayashi, S., Carpenter, K., Suzuki, D., 2009. Differente growth patterns between the skeleton and osteoderms of *Stegosaurus* (Ornithischia: Thyreophora). Journal of Vertebrate Paleontology 29, 123–131.

Hayashi, S., Carpenter, K., Scheyer, T.M., Watabe, M., Suzuki, D., 2010. Function and evolution of ankylosaur dermal armor. Acta Palaeontologica Polonica 55, 213–228.

Hubert, J.F., Panish, P.T., Chure, D.J., Prostak, K.S., 1996. Chemistry, microstructure, petrology, and diagenetic model of Jurassic dinosaur bones, Dinosaur National Monument, Utah. Journal of Sedimentary Research 66, 531–547.

Jackson, F.D., Horner, J.R., Varricchio, D.J., 2010. A study of a *Troodon* egg containing embryonic remains using epifluorescence microscopy and other techniques. Cretaceous Research 31, 255–262.

Jarvis, I., 1992. Sedimentology, geochemistry and origin of phosphatic chalks: the Upper Cretaceous deposits of NW Europe. Sedimentology 39, 55–97.

Klein, N., Sander, P.M., 2008. Ontogenetic stages in the long bone histology of sauropod dinosaurs. Paleobiology 34, 247–263.

Kremer, B., Owocki, K., Królikowska, A., Wrzosek, B., Kazmierczak, J., 2012. Mineral microbial structures in a bone of the Late Cretaceous dinosaur *Saurolophus angustirostris* from the Gobi Desert, Mongolia - a Raman spectroscopy study. Palaeogeography, Palaeoclimatology, Palaeoecology 358–360, 51–61.

Moreno-Azanza, M., Canudo, J.I., Gasca, J.M., 2014. Unusual theropod eggshells from the Early Cretaceous Blesa formation of the Iberian range, Spain. Acta Paleontologica Polonica 59, 843–854.

Merino, L., Buscalioni, A.D., 2013. Mineralogía y cambios composicionales en fragmentos óseos atribuidos a un dinosaurio ornitópodo del yacimiento barremiense de Buenache de la Sierra (Formación Calizas de La Huérguina, Cuenca, España). Estudios Geológicos, 69, 193–207.

Organ, C. L., Adams, J., 2005. The histology of ossified tendon in dinosaurs. Journal of Vertebrate Paleontology 25(3), 602–613.

Ortega, F., Escaso, F., Gasulla, J.M., Dantas, P., Sanz, J.L., 2006. Dinosaurios de la Península Ibérica. Estudios Geológicos 62, 219–240.

Padian, K., Lamm, E.-T., 2013. Bone Histology of Fossil Tetrapods: Advancing Methods, Analysis and Interpretation. University of California Press, Berkeley and Los Angeles, 285 pp.

Parenteau, M.N., Cady, S.L., 2010. Microbial biosignatures in iron-mineralized phototrophic mats at Chocolate Pots Hot springs, Yellowstone National Park, United States. Palaios 25, 97–111.

Pereda-Suberbiola, X., Ruiz-Omeñaca, J. I., Canudo, J. I., Torcida, F., Sanz, J. L., 2012. Dinosaur faunas from the Early Cretaceous (Valanginian-Albian) of Spain. In: Godefroit, P. (Ed.), Bernissart dinosaurs and Early Cretaceous terrestrial ecosystems. Indiana University Press, Bloomington, pp. 379–407.

Perales-Gogenola, L., Pereda-Suberbiola, X., Canudo, J.I., 2018. Palaeohistological characterization of the ornithischian dinosaur remains from the Lower Cretaceous

(Barremian) of La Cantalera (Josa, Teruel, Iberian Peninsula). In: Amayuelas, E., Bilbao Lasa, P., Bonilla, O., del Val, M., Errandonea-Martin, J., Garate-Olave, I., García-Sagastibelza, A., Intxauspe-Zubiaurre, B., Martinez-Braceras, N., Perales-Gogenola, L., Ponsoda-Carreres, M., Portillo, H., Serrano, H., Silva-Casal, R., Suárez-Bilbao, A., Suarez-Hernando, O. (Eds.), Life finds a way, Libro de Resúmenes del XVI Encuentro de Jóvenes Investigadores en Paleontología / Abstract Book of the XVI Meeting of Young Researchers in Paleontology, Zumaia, pp. 91–94.

Pinheiro, F.L., Horn, B.L.D., Schultz, C.L., de Andrade, J.A.F.G., Sucerquia, P.A., 2012. Fossilized bacteria in a Cretaceous pterosaur headcrest. Lethaia 45, 495–499.

Pfretzschner, H.U., 2000. Microcracks and fossilization of Haversian bone. Neues Jahrbuch für Geologie und Paläontologie Abhandlungen 216, 413–432.

Pfretzschner, H.U., 2001. Iron oxides in fossil bone. Neues Jahrbuch für Geologie und Paläontologie Abhandlungen 220, 417–429.

Pfretzschner, H.U., 2004. Fossilization of Haversian bone in aquatic environments. Comptes Rendus Palevol 3, 605–616.

Riveline, J., Berger, J.P., Feist, M., Martín-Closas, C., Schudack, M., Soulié-Märsche, I., 1996. European Mesozoic–Cenozoic charophyte biozonation. Bulletin de la Société géologique de France 167, 453–468.

Rogers, R., Brady, M., 2010. Origins of microfossil bonebeds: insights from the Upper Cretaceous Judith River Formation of north-central Montana. Paleobiology 36, 80–112.

Rosales, I., Pomar, L., Al-Awwad, S.F., 2018. Microfacies, diagenesis and oil emplacement of the Upper Jurassic Arab-D carbonate reservoir in an oil field in central Saudi Arabia (Khurais Complex). Marine and Petroleum Geology 96, 551–576.

Ruiz-Omeñaca, J.I., 2011. *Delapparentia turolensis* nov. gen et sp., un nuevo dinosaurio iguanodontoideo (Ornithischia: Ornithopoda) en el Cretácico Inferior de Galve. Estudios Geológicos 67, 83–110.

Ruiz-Omeñaca, J.I., Canudo, J.I., Cuenca-Bescós, G., 1997. Primera evidencia de un área de alimentación de dinosaurios herbívoros en el Cretácico Inferior de España (Teruel). Monografías de la Real Academia de Ciencias Exactas, Físicas, Químicas y Naturales de Zaragoza 10, 1–48.

Russo, F., Gautret, P., Mastandrea, A., Perri, E., 2006. Syndepositional cements associated with nannofossils in the Marmolada Massif: evidences of microbially mediated primary marine cements? (Middle Triassic, Dolomites, Italy). Sedimentary Geology 185, 267-–275.

Sander, P.M., Mateus, O., Laven, T., Knötschke, N., 2006. Bone histology indicates insular dwarfism in a new Late Jurassic sauropod dinosaur. Nature 441, 739–741.

Scheyer, T.M., Sander, P.M., 2004. Histology of ankylosaur osteoderms: Implications for systematics and function. Journal of Vertebrate Paleontology 24, 874–893.

Schwertmann, U., Murad, E., 1983. Effect pH on the formation of goethite and hematite from ferrihydrite. Clays and Clay Minerals 31, 277–284.

Sereno, P.C., 1997. The origin and evolution of dinosaurs. Annual Review of Earth and Planetary Sciences 25, 435–489.

Timlin, J.A., Carden, A., Morris, M.D., Rajachar, R.M., Kohn, D.H., 2000. Raman spectroscopic imaging markers for fatigue-related microdamage in bovine bone. Analytical Chemistry 72, 2229–2236.

Toporski, J.K.W., Steele, A., Westall, F., Avci, R., Martill, D.M., McKay, D.S., 2002. Morphologic and spectral investigation of exceptionally well-preserved bacterial biofilms from the Oligocene Enspel formation, Germany. Geochimica et Cosmochimica Acta 66, 1773–1791.

Trueman, C.N., 1999. Rare Earth Element Geochemistry and Taphonomy of Terrestrial Vertebrate Assemblages. Palaios 14, 555–568.

Vickaryous, M.K., Hall, B.K., 2008. Development of the dermal skeleton in *Alligator mississippiensis* (Archosauria, Crocodylia) with comments on the homology of osteoderms. Journal of Morphology 269, 398–422.

Vickaryous, M.K., Russell, A.P., Currie, P.J., 2001. Cranial ornamentation of ankylosaurs (Ornithischia: Thyreophora): Reappraisal of developmental hypotheses. In: Carpenter, K. (Ed.), The Armored Dinosaurs. Indiana University Press, Bloomington and Indianapolis, pp. 318–340.

Walrafen, G.E., Chu, Y.C., 2000. Nature of collagen-water hydration forces: a problem in water structure. Chemical Physics 258, 427–446.

Wedel, M. J., Cifelli, R.L., Sanders, R. K., 2000. Osteology, paleobiology, and relationships of the sauropod dinosaur *Sauroposeidon*. Acta Palaeontologica Polonica 45, 343-388.

Zweers, G. A., Vanden Berge, J. C., Koppendraier, R., 1987. Avian cranio-cervical system Part I: anatomy of the cervical column in the chicken (*Gallus gallus* L.). Acta Morphologica Neerlands-Scandinavia 25, 135-155.

Caption of the figures and tables

Figure 1. Geographical and geological location of La Cantalera-1 site (Lower Cretaceous, Teruel, Spain). A: Stratigraphical setting of the Blesa Formation. B: Location of La Cantalera-1 site within the Blesa Formation section. C: Simplified geologic map of the Iberian

Peninsula, palaeogeographic sub-basins (Ol: Oliete, Pa: Las Parras, Ga: Galve, Mo: Morella, Pe: Perelló, Sa: Salzedella, Pg: Peñagolosa) within the Maestrazgo Basin and active faults during Early Cretaceous sedimentation and geographical location of La Cantalera-1 site near the village of Josa, Teruel province. Modified from Canudo et al. (2010).

Figure 2. Palaeohistological features seen in the fossil bones of Ornithopoda indet. from the La Cantalera-1 site (Teruel, Spain) with transversal orientation. A: Vertebra (MPZ 2018/501) in transverse view with multiple layers forming the external cortical complex and secondary osteons. Scale bar: 0.5 mm. B: External portion of the compact bone of the vertebra (MPZ 2018/495), showing a thin avascular external layer. Scale bar: 1 mm. C: Small vertebra (MPZ 2018/494) with lamellar matrix and multiple primary osteons and blood vessels. Scale bar: 0.5 mm. D: Transition between compact bone and the trabecular bone of the vertebra (MPZ 2018/495), with wider cavities covered by red oxides. Crossed Nicols. Scale bar: 1 mm. E: Rib (MPZ 2018/493) showing scarce vascularization and external cortex with slight lamination. Scale bar: 0.5 mm. F: Trabecular bone of the rib (MPZ 2018/493) with great cavities covered by red iron oxides. Scale bar: 0.5 mm. G: Rib (MPZ 2018/499) with extremely abundant longitudinal vascularization and two different colorations (1 and 2) that may correspond to cyclical growth. Scale bar: 1 mm. H: Trabecular bone of the rib (MPZ 2018/499). Trabecular cavities completely covered by red iron oxides. Crossed Nicols. Scale bar: 1 mm.

Figure 3. Palaeohistological features seen in the fossil bones of Ornithopoda indet. from the La Cantalera-1 site (Teruel, Spain) with transversal orientation. A: Great abundance of blood vessels and primary osteons in the compact bone of the rib (MPZ 2018/492). Scale bar: 0.2 mm. B: Abrupt transition between compact bone with great vascularization and trabecular

bone with wider cavities in the rib MPZ 2018/492. Scale bar: 0.2 mm. C-D: Fibula (MPZ 2018/502) in transverse view with parallel (F) and crossed Nicols (G) showing a lax Haversian bone structure. Scale bars: 1 mm. E: Transition between the compact bone and trabecular bone of the fibula (MPZ 2018/502), less abrupt than in the rib (MPZ 2018/492) and with greater trabeculae. Scale bar: 1 mm. F: Ossified tendon (MPZ 2018/491) in transverse view presenting dense Haversian bone structure with secondary osteons overlapping one another. Scale bar: 0.5 mm.

Figure 4. Palaeohistological features seen in the dermal bones of Ankylosauria indet. from the La Cantalera-1 site (Teruel, Spain) with transversal orientation. A-D: Dermal ossicle (MPZ 2018/508) in transverse view, external cortex seen with parallel (A) and crossed Nicols (B), and internal morphology with parallel (C) and crossed Nicols (D). The ossicle is mainly formed of collagen structural fibres, seen arranged in three different orientations (1, 2 and 3) both in the cortex area (A, B) and in the internal area (C, D). E: Cortex features of dermal ossicle (MPZ 2018/507) with crossed Nicols, a blood vessel (4) opening to the surface of the ossicle. F: Inner features of the basal part of a dermal scute (MPZ 2018/505) with crossed Nicols, showing a structure with more osteons and small trabeculae and fewer collagen structural fibres than the ossicles. G: Small dermal spine (MPZ 2018/503) with a skeletal bone-like inner structure without the great organization of the collagen structural fibres. H: Basal part of a small dermal spine (MPZ 2018/504) with small trabeculae and some collagen structural fibres. Scale bars: 1 mm.

Figure 5. Microstructure of Ornithopoda fossil bones from the La Cantalera-1 site (Teruel, Spain) with transversal orientation. A: microstructure of compact bone with densely packed Haversian systems stained in pink tones by Alizarin Red S. The small fractures (indicated by

the green arrow heads) are bleached. The Haversian channels are completely occupied by opaque ore (goethite). Parallel Nicols. Scale bar: 0.5 mm. B: the same image as A, with a visibly high density of secondary osteons. Crossed Nicols. Scale bar: 0.5 mm. C-D: passage from compact bone tissue to cancellous (trabecular) tissue. The filling of the Haversian and Volkmann channels comprises a clean carbonate in the compact tissue, whereas in the cancellous tissue the opaque ore is regularly relieved by two carbonate phases (1, 2) until the trabecular spaces are completely occupied. Parallel and crossed Nicols. Scale bar: 0.5 mm. E-F: detail of the trabecular space filled by a goethite phase and two different phases (1 and 2) of calcite. Parallel and crossed Nicols. Scale bar: 1 mm. G-H: general view and detail of the opaque phase with a nucleus that suggests a goethite (g) composition, changing to altered hematite (h). Crossed Nicols. Scale bars: G: 1 mm, H: 0.2 mm.

Figure 6. Fractures and process of replacement in the microstructure of Ornithopoda fossil bones from the La Cantalera-1 site (Teruel, Spain) with transversal orientation. A: fragile fractures pointed out by green arrow heads, with thin replacement veins formed by remobilization of the phosphatic phase (francolite). Parallel Nicols. Scale bars: 1 mm. B: open fracture, with iron oxide replacement that advances laterally towards the interior. Parallel Nicols. Scale bars: 1 mm. C: cancellous tissue, affected by the intense early compaction, with the accumulation of angular fragments. Parallel Nicols. Scale bars: 1 mm. D: thin phase of opaque ore (goethite), with a growth towards the central zone of the hollow, followed by a filling of two differentiated carbonated phases; the first one (1) of clean spatial crystals, and the second one (2) with insoluble iron oxides together with organic remains. Scale bars: 0.5 mm. E-H: general appearance of mineralized cancellous bone showing a replacement phase of iron oxides in concentric bands. G-H: details of the bone replacement process with abrupt interruptions of the advance front. Staining with Alizarin Red S. E and G with parallel Nicols, F and H with crossed Nicols. Scale bars: E-F: 1 mm and G-H: 0.5 mm.

Figure 7. Microstructure of Ankylosauria fossil bones from the La Cantalera-1 site (Teruel, Spain). A-B: compact tissue with bands of fibres parallel to each other, which intersect perpendicularly as a network with the scattered Volkmann channels occupied with calcite and opaque ore crystals. It shows a generalized pink-coloured tone (p), with a subsequent bleaching stage (b) favoured by the presence of very fine fractures. Staining with Alizarin Red S, parallel and crossed Nicols, respectively. Thin sections with lateral orientation. C-F: general view and details where small fractures are observed; the filling of the empty spaces in the cancellous tissue is mostly carbonated (1 and 2 phases), with just a remnant of the earliest phase of iron oxides. Thin sections with transversal orientation. Parallel (C, E) and crossed (D, F) Nicols. Scale bars: 1 mm.

Figure 8. Different views under cathodoluminescence (CL) and epifluorescence (UVF) of Ornithopoda fossil bones from the La Cantalera-1 site (Teruel, Spain). A-D: compact and cancellous tissues are not luminescent under CL. In the filling, the earliest carbonated phase formed by large crystals of clean equant calcite is shown by a non-luminescent dark zone with straight rectilinear faces, followed by alternating reddish and yellow laminar growth and finally by a larger irregular area of yellowish tones. In the last carbonated phase, formed by dirty calcite crystals with inclusions of insoluble remains, the luminescence is massively reddish, but not intense, with some yellow areas irregularly arranged and of small size. A and C parallel Nicols; B and D under CL. E-F: under UVF the bone periphery and fracture zones show a strong light blue luminescence that advances towards the interior of the bone. The filling of the trabecular spaces with goethite appears inert whereas the filling formed by clean calcite crystals (first phase) is luminescent, with an intense dark blue tone. The dirty calcite (second phase) appears as non-luminescent with some points irregularly distributed in a blue

tone. Parallel Nicols and UVF, respectively. G-H: the bone structure may undergo a greater degree of alteration, leaving the entire surface practically in a light blue tone, whereas the remaining part remains in a dark violet colour. Thin sections with transversal orientation. Scale bars: A-D: 0.5 mm; E-H: 0.2 mm.

Figure 9. Different views by scanning electron microscope (SEM) of the microstructure of the bone and filling of Ornithopoda fossil bones from the La Cantalera site (Teruel, Spain). A-B: general view and detail in the collagen zone, which shows the presence of spherical bodies ranging in size from 100 to 300 nm, as possible relicts of nanobacterial cells. Scale bars: A: 20 mm, B: 3 mm. C-D: general view and detail of the contacts, marked by black lines, among compact bone (b), goethite (g) and calcite phase (c) fillings. Scale bars: C: 100 mm, D: 30 mm~~m~~. E: detail of the contact between fibro-radial goethite (g) crystals and large equant calcite crystals. Scale bar: 10 mm. F: detail view showing the massive organic coccoid carpets together with a filament with helicoidal fissures (*Gallionella*-like bacteria). Scale bar: 20 mm. G-H: general view and detail of the idiomorphic calcite crystals (second phase) associated with bacterial activity (coccoid carpets and filaments). Scale bars: G: 100 mm, H: 20 mm.

Table 1. Ornithischian dinosaur material from the Lower Cretaceous of La Cantalera (Teruel, Spain) included in this study.

Table 2. Francolite X-ray data from phosphatic chalks (Jarvis, 1992) used as a standard together with corresponding values from the fossil bones of ankylosaurian (MPZ 2017/504; MPZ 2018/506) and ornithopod dinosaurs (MPZ 2018/493) from La Cantalera (Teruel). The peaks, identified by their interplanar spacings in Angstroms (A) and relative intensity (I/I0), are consistent with a well-crystallized francolite. Goethite (*), quartz (**) and calcite (***)

are minor constituents (in red colour). In bold type, the peak more characteristic of the francolite (I/Io=100). Data published by the International Centre for Diffraction Data (ICDD). * Goethite 29-713; ** Quartz 33-1161.

Specimen nb.	**Taxon**	**Type of fossil remain**
MPZ 2018/491	Ornithopoda indet.	Ossified tendon
MPZ 2018/492	Ornithopoda indet.	Rib
MPZ 2018/493	Ornithopoda indet.	Rib
MPZ 2018/494	Ornithopoda indet.	Small vertebra
MPZ 2018/495	Ornithopoda indet.	Neural arch
MPZ 2018/496	Iguanodontoidea indet.	Ulna
MPZ 2018/497	Ornithopoda indet.	Proximal rib
MPZ 2018/498	Ornithopoda indet.	Ossified tendon
MPZ 2018/499	Ornithopoda indet.	Rib
MPZ 2018/500	Ornithopoda indet.	Dorsal vertebra
MPZ 2018/501	Ornithopoda indet.	Vertebra
MPZ 2018/502	Ornithopoda indet.	Fibula
MPZ 2018/503	Ankylosauria indet.	Small dermal spine
MPZ 2018/504	Ankylosauria indet.	Small dermal spine (basal part)
MPZ 2018/505	Ankylosauria indet.	Dermal scute (basal part)
MPZ 2018/506	Ankylosauria indet.	Dermal ossicle
MPZ 2018/507	Ankylosauria indet.	Dermal ossicle
MPZ 2018/508	Ankylosauria indet.	Dermal ossicle
MPZ 2018/509	Ankylosauria indet.	Dermal scute
MPZ 2018/510-512	Ankylosauria indet.	Dermal scute (fragments)

	FRANCOLITE In Jarvis (1992)		**DINOSAUR** Sample 622 (Elorza et al., 1999)		**DINOSAUR** Sample MPZ 2018/504		**DINOSAUR** Sample MPZ 2018/506		**DINOSAUR** Sample MPZ 2018/493	
d(A)	I/I0	hkl	d(A)	I/I0	d(A)	I/I0	d(A)	I/I0	d(A)	I/I0
8.08	6	100	7.848	3.3	8.08	8	8.11	4	8.23	7
					4.19*		4.19*		4.19*	
4.04	6	200	4.029	3	4.06	3	4.04	4	4.07	4
3.87	6	111	3.848	4	3.86	4	3.85	7	3.89	9
3.45	45	2	3.427	29.7	3.44	49	3.44	43	3.45	66
			3.321**	4.9						
3.17	16	102	3.153	9.7	3.17	11	3.17	11	3.17	16
3.05	18	120; 210	3.041	12.7	3.07	16	3.06	15	3.07	11
							3.04***		3.04***	
2.79	**100**	212; 211	2.785	**100**	**2.80**	**100**	**2.80**	**100**	**2.8**	**100**
2.77	55	112	2.757	64.5	2.78	71	2.77	44	2.78	71
2.69	50	300	2.684	54.4	2.70	79	2.70	54	2.7	70
2.62	30	202	2.610	22.2	2.62	29	2.62	22	2.63	20
2.51	4	301	2.498	4.5	2.51	8	2.51	4	2.52	18
			2.443*	2.8	2.44*		2.44*		2.44*	
2.28	8	122; 212	2.275	8.5	2.29	5	2.29	7		
2.24	20	130; 310	2.234	22.6	2.25	28	2.25	23	2.25	33
2.13	6	131; 311	2.121	6.5	2.13	8	2.13	4	2.13	4
2.06	6	113	2.058	4.9	2.06	6	2.06	4	2.06	8
2.02	2	126B								
1.998	4	203	1.972	13	1.999	4	1.998	4	2	6
1.931	25	222	1.929	21.4	1.937	30	1.934	23	1.938	24
1.878	12	132; 312	1.878	11.6	1.878	11	1.886	8	1.886	10
1.836	30	123; 213	1.833	25	1.837	33	1.837	27	1.839	35

1.789	12	231; 321	1.790	13.6	1.796	15	1.795	10	1.799	16
1.762	10	140; 410	1.762	13.9	1.772	13	1.767	8	1.772	6
1.742	10	402	1.739	11.3	1.745	12	1.747	9	1.751	6
1.724	16	4	1.718	14.5	1.722	23	1.772	17	1.772	22
1.632	4	232; 322	1.629	4.5	**		**			
1.604	2	133; 313	1.602	2.1	1.607	3	1.602	4		

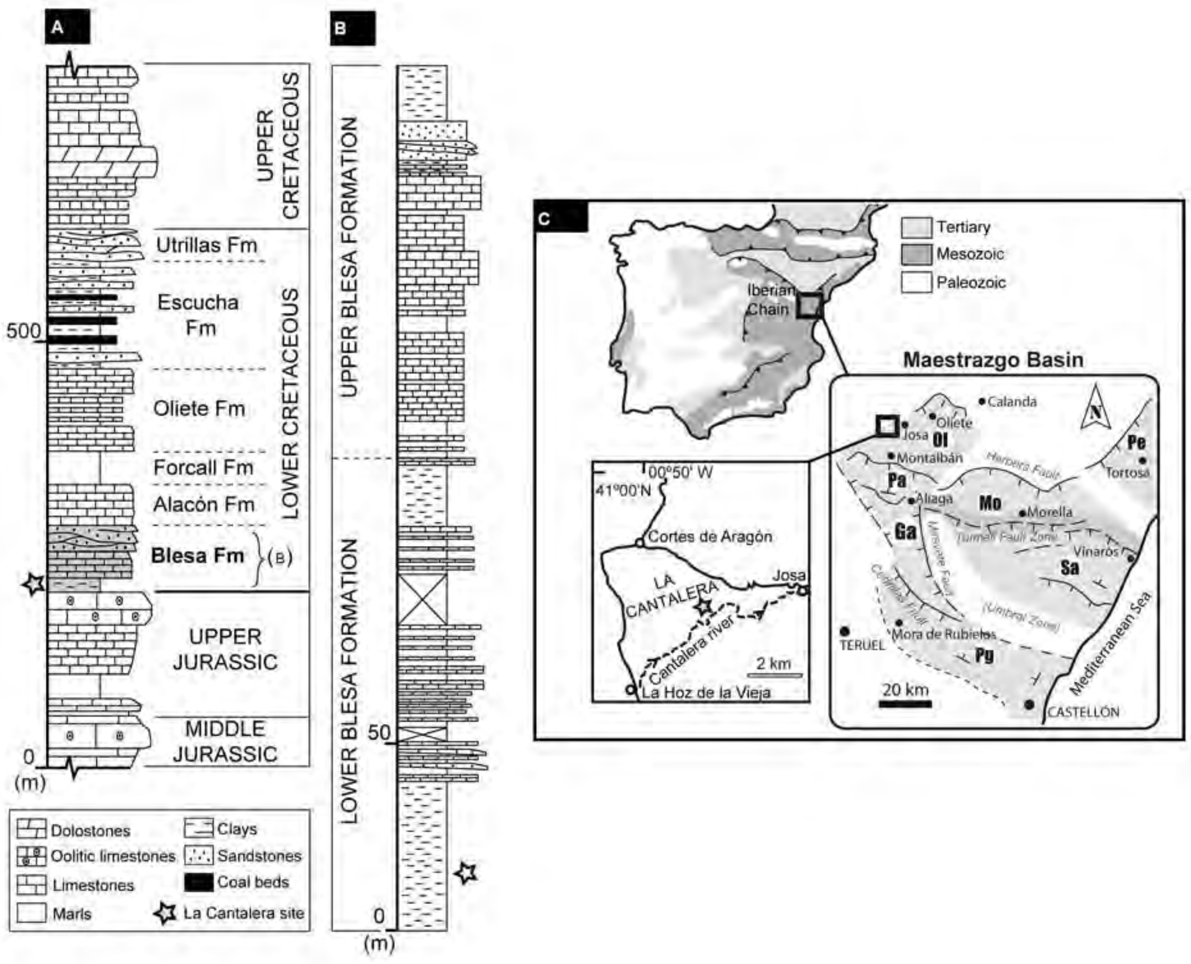
A
UPPER CRETACEOUS
Utrillas Fm
Escucha Fm
500
Oliete Fm
Forcall Fm
Alacón Fm
Blesa Fm
(B)
LOWER CRETACEOUS
UPPER JURASSIC
MIDDLE JURASSIC
0
(m)
Dolostones
Oolitic limestones
Limestones
Marls
Clays
Sandstones
Coal beds
La Cantalera site
B
UPPER BLESA FORMATION
LOWER BLESA FORMATION
50
0
(m)
C
Tertiary
Mesozoic
Paleozoic
Iberian Chain
Maestrazgo Basin
Calanda
Oliete
Josa
Ol
Montalbán
Pa
Aliaga
Mo
Morella
Pe
Tortosa
Herbers Fault
Turmell Fault Zone
Vinaròs
Sa
Ga
Miravete Fault
Cedrillas Fault
(Umbral Zone)
Mora de Rubielos
TERUEL
Pg
20 km
CASTELLÓN
Mediterranean Sea
N
00º50' W
41º00'N
Cortes de Aragón
LA CANTALERA
Josa
Cantalera river
2 km
La Hoz de la Vieja

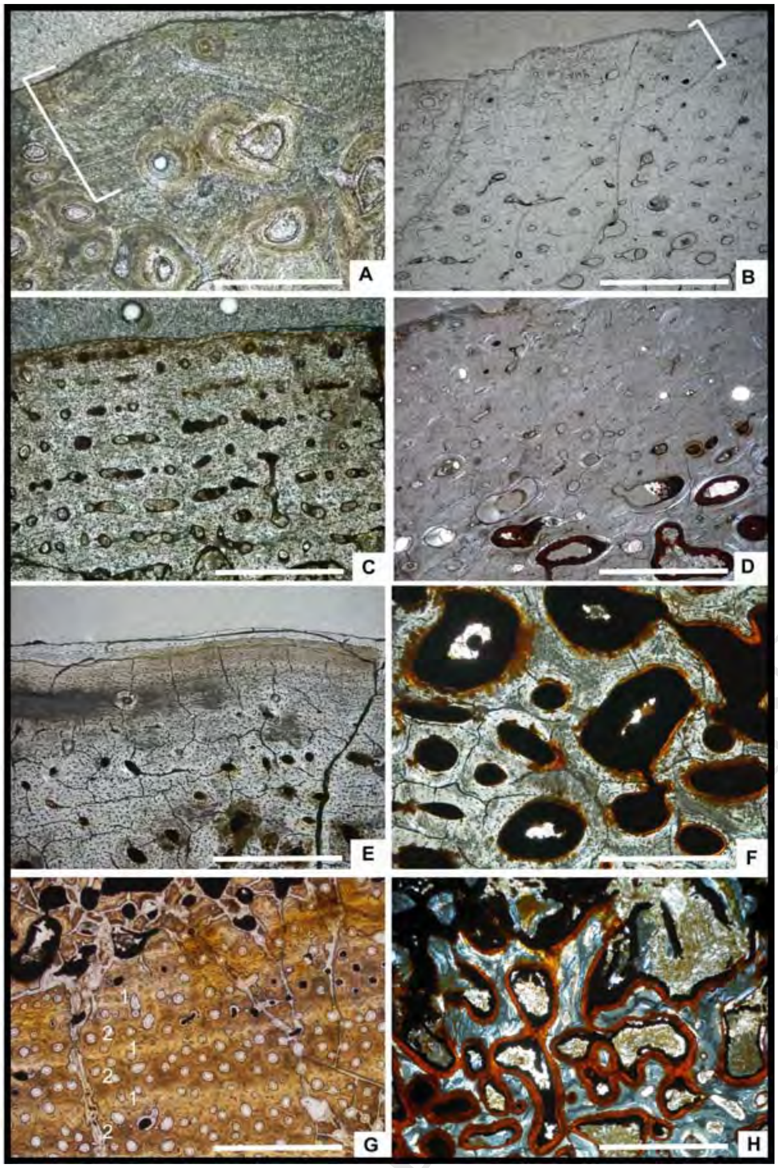
A
B
C
D
E
F
1
2
1
2
1
2
G
H

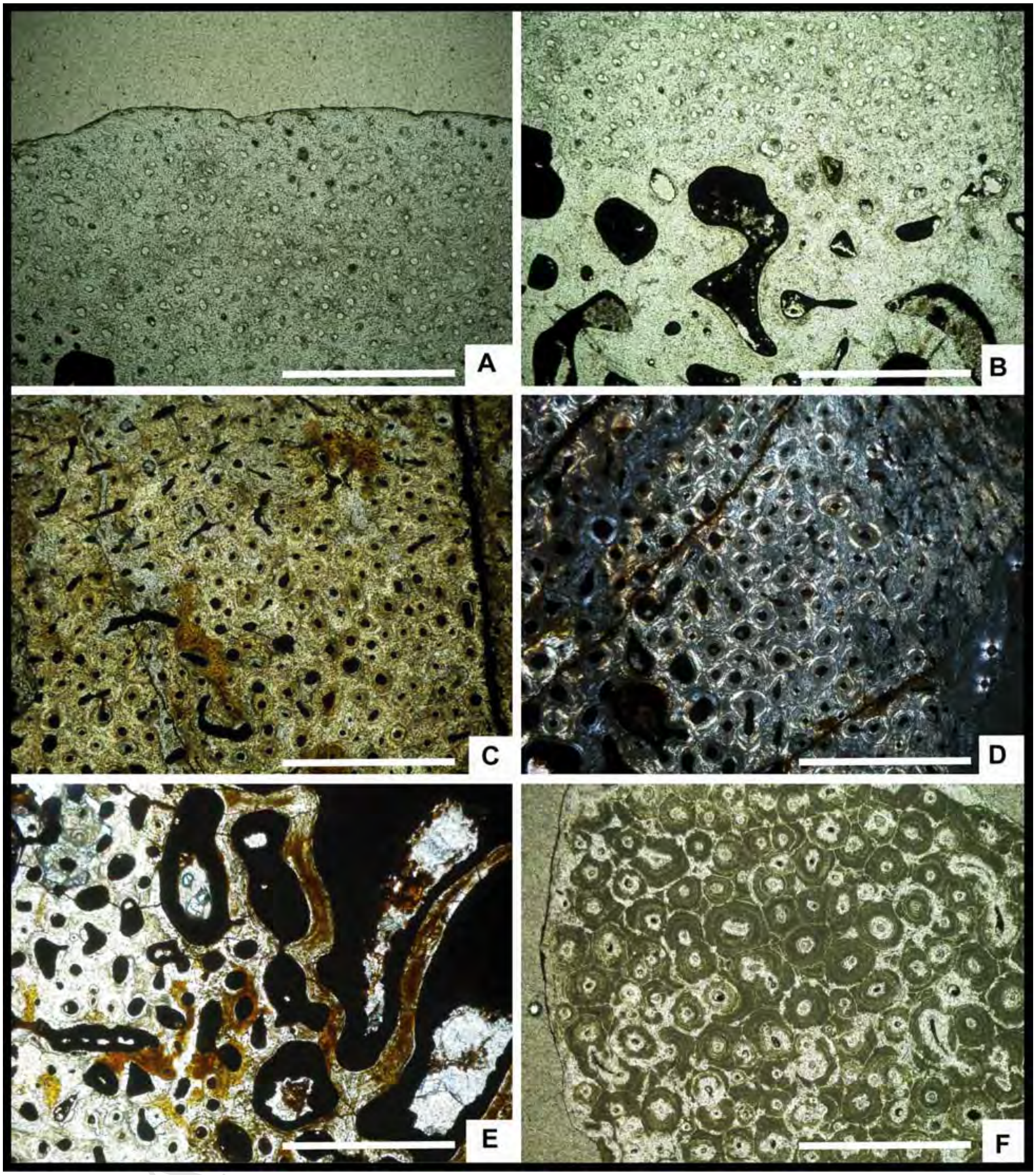
A
B
C
D
E
F

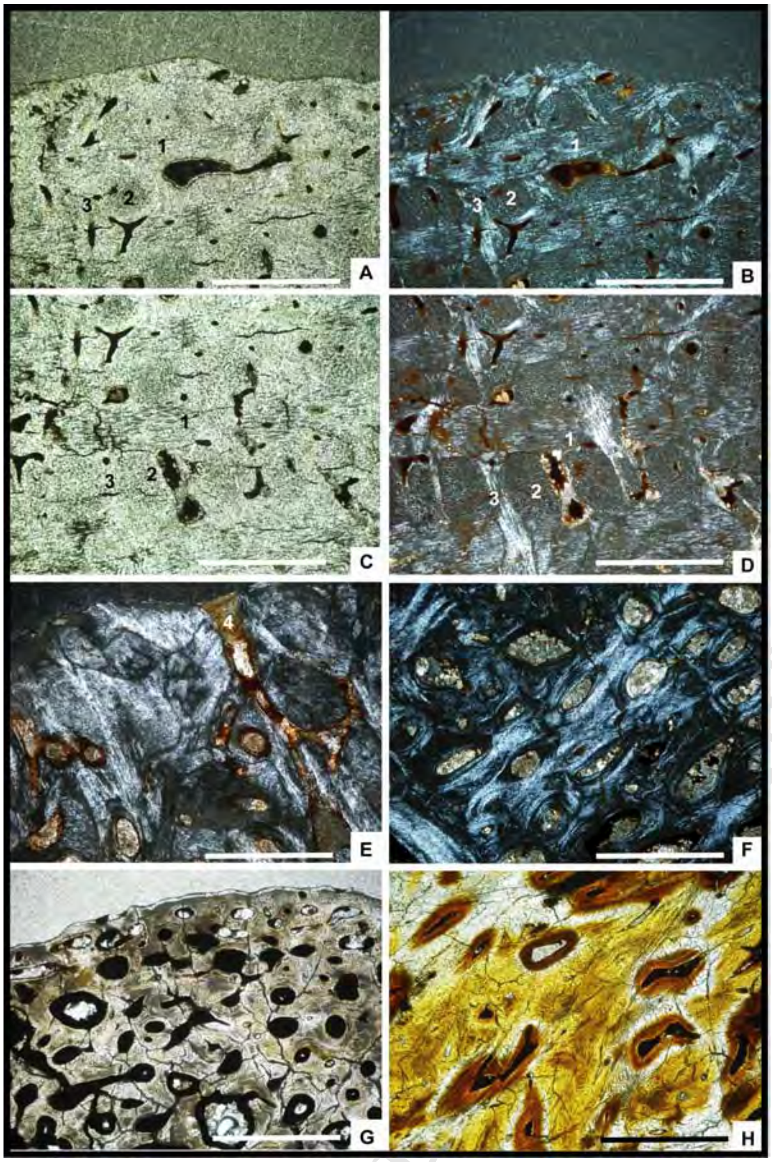
1
2
3
A
1
2
3
B
1
2
3
C
1
2
3
D
4
E
F
G
H

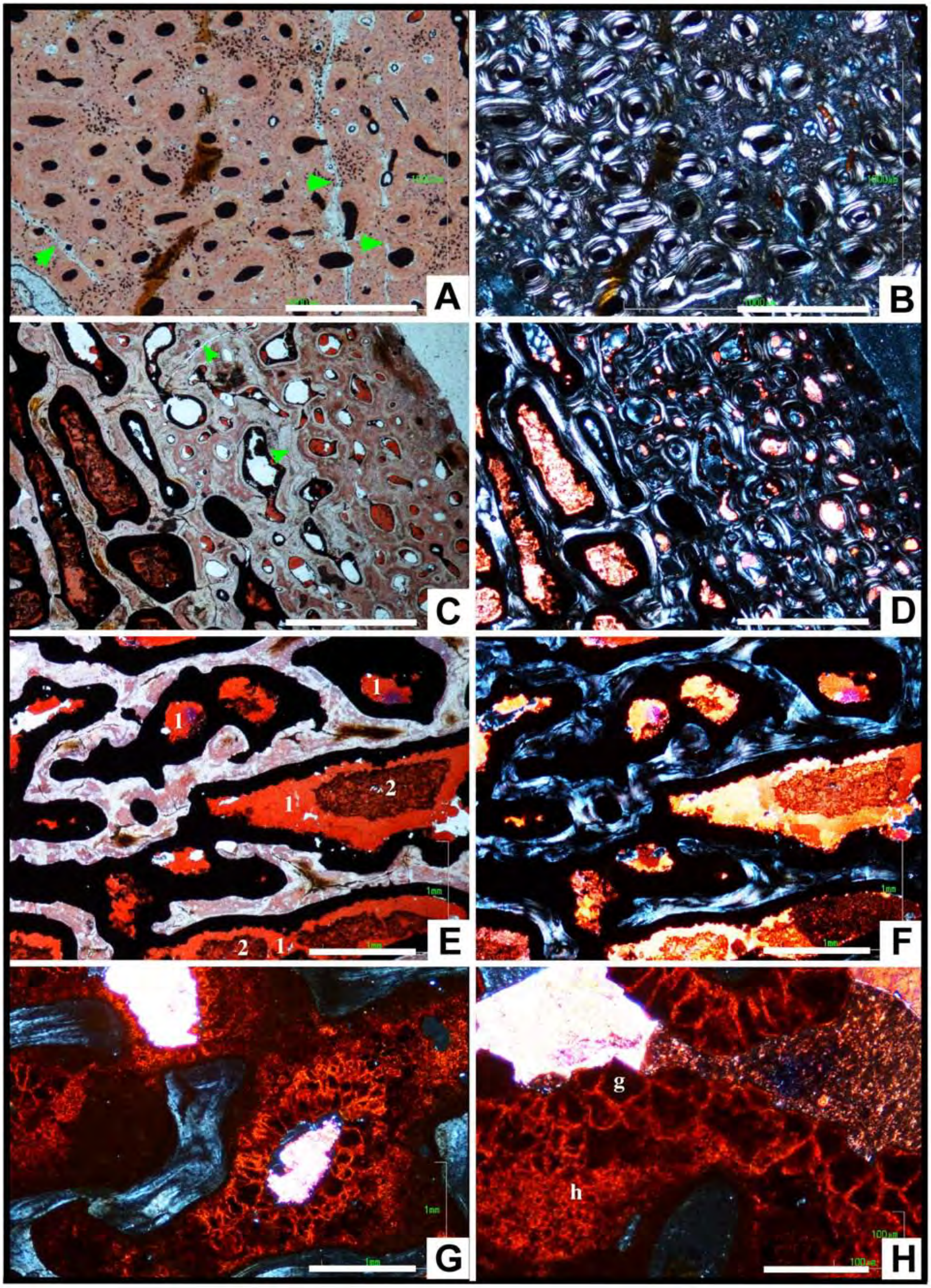
A
B
C
D
1
1
1
2
1
2
1
1mm
1mm
E
1mm
1mm
F
1mm
1mm
G
g
h
100 µm
100 µm
H

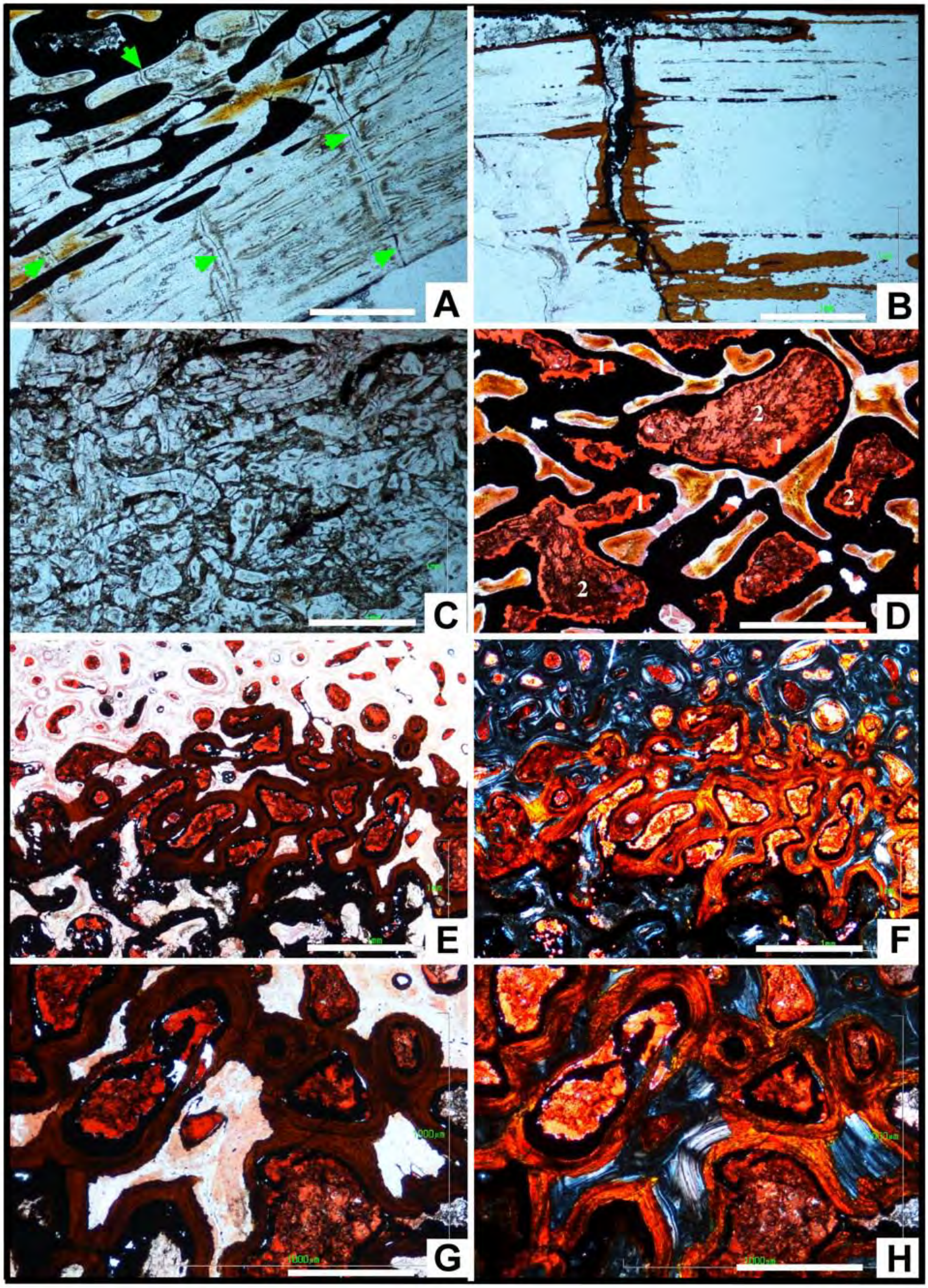
A
B
C
1
2
1
1
2
2
D
1mm
E
1mm
F
1000µm
G
1000µm
H

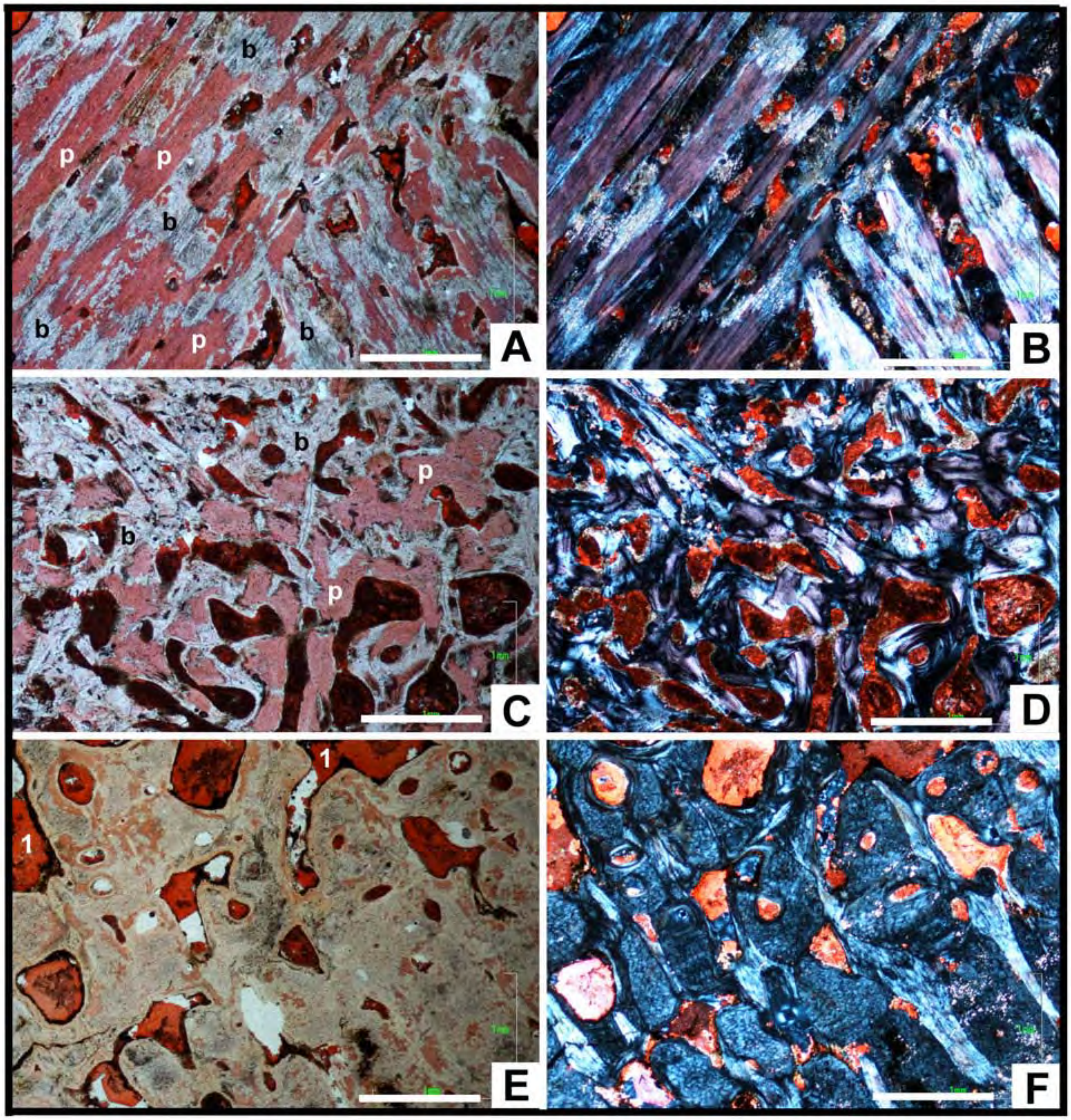
b
p
p
b
b
p
b
A
B
b
p
b
p
C
D
1
1
E
F

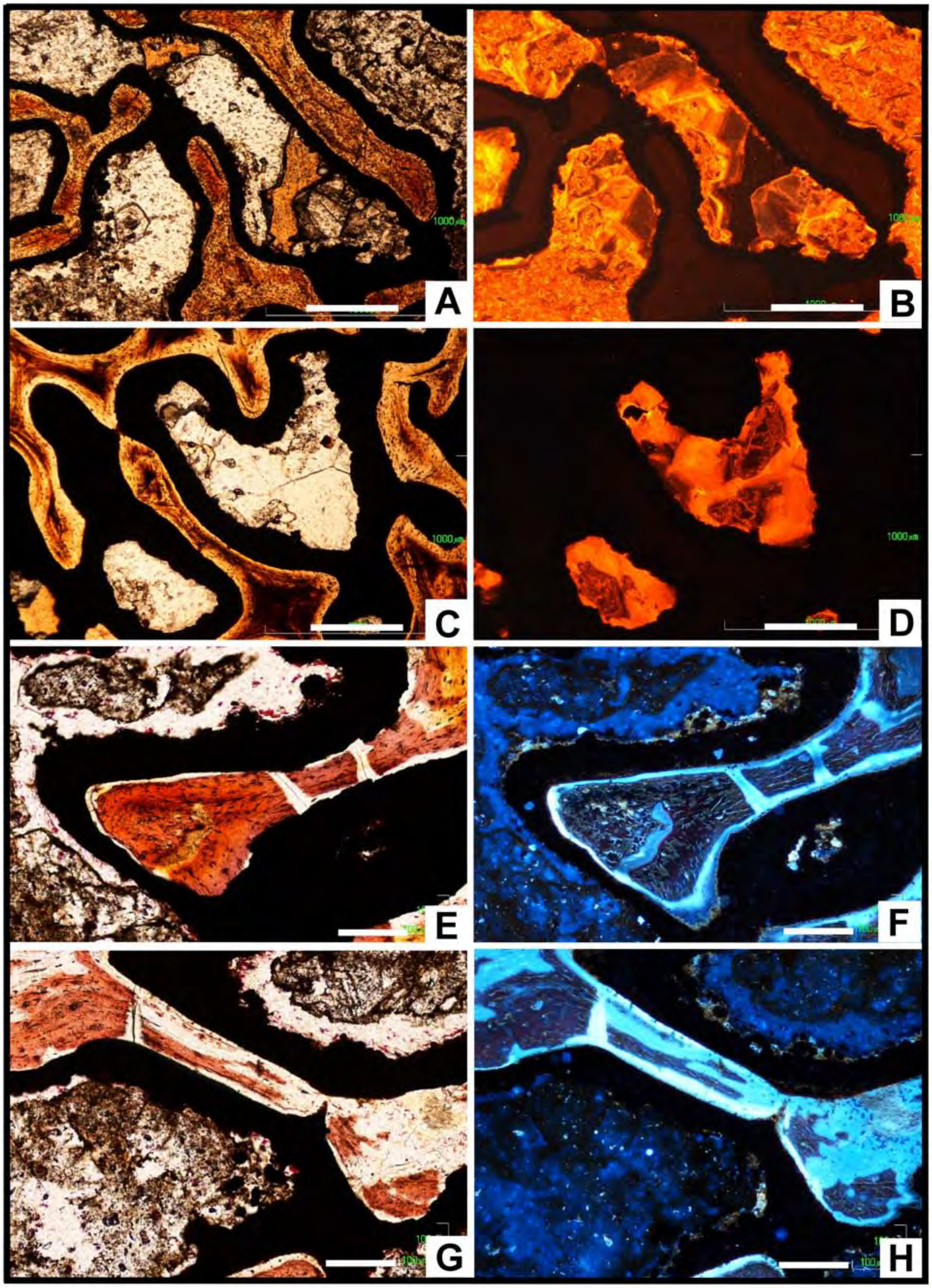
A
B
C
D
E
F
G
H
1000µm
1000µm
1000µm
1000µm

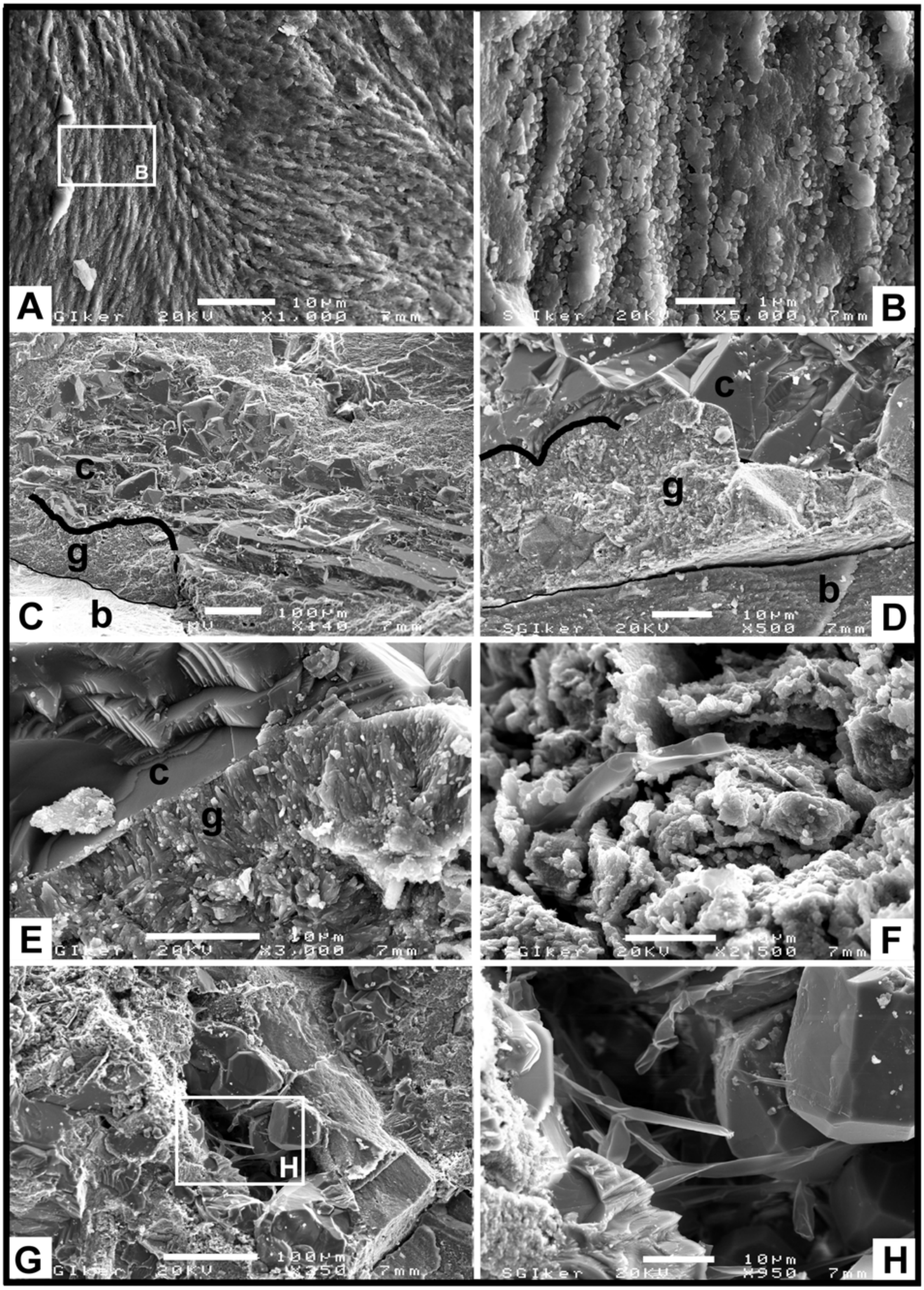
B
A
10µm
GIker 20KV X1,000 7mm
1µm
SGIker 20KV X5,000 7mm
B
c
g
C
b
100µm
X140 7mm
c
g
b
10µm
SGIker 20KV X500 7mm
D
c
g
E
10µm
GIker 20KV X3,000 7mm
10µm
SGIker 20KV X2,500 7mm
F
H
G
100µm
GIker 20KV X350 7mm
10µm
SGIker 20KV X950 7mm
H

Highlights

- First palaeohistological study of Ornithischia from La Cantalera-1 (Spain).
- Presence of *Polacanthus*-like ankylosaur suggested by histological features of osteoderms.
- Mineral fill suggests the dinosaur bones underwent rapid burial in a phreatic environment.
- Evidence of microbial (nanobacterial) participation, possibly favouring fossilization.